Articles

Contribution from the Department of Chemistry,
The University of Texas at Austin, Austin, Texas 78712

Complexation of the Nickel(II) Triad with 14-Membered Macrocyclic $P_{4-n}S_n$ (n = 2, 1, 0) Ligands. Study of the Effects on Coordination of the Relative Configuration at the Phosphines and the Number and Placement of Thioether Sites[1]

Evan P. Kyba,* Raymond E. Davis,* Marye Anne Fox,* Clyde N. Clubb, Shiuh-Tzung Liu,
Gary A. Reitz, Victor J. Scheuler, and Ram P. Kashyap

Received September 4, 1986

Complexes of the nickel(II) triad formed from the following 14-membered macrocyclic ligands were prepared and characterized: 2,6,13,17-tetraheteratricyclo[16.4.0.0^{7,12}]docosa-7(12),8,10,1(18),19,21-hexaene; hetera = 2,13-dithia and *cis*- and *trans*-6,17-diphenyldiphospha, *c*- and *t*-PSPS, respectively; hetera = 2,6-dithia and *cis*- and *trans*-13,17-diphenyldiphospha, *c*- and *t*-PSSP, respectively; hetera = 2,17-dithia and *cis*-6,13-diphenyldiphospha, *c*-P_2S_2; hetera = 2-thia and *cis,cis*- and *trans,trans*-6,13,17-triphenyltriphospha, *c*- and *t*-P_3S, respectively; hetera = *cis,cis,cis*-2,6,13,17-tetraphenyltetraphospha, *c*-P_4. Molar conductivities and UV–vis and ^{31}P NMR spectroscopies were particularly useful in determining solution-phase structures. Crystal structures were determined for five complexes. The effect of ligand environment on the redox properties of the bound metal ion was studied by cyclic voltammetry. The coordinating ability of the macrocyclic ligands was determined by solution-phase competition experiments and found to depend on the metal species, the nature, number and disposition in the ring of the heteroatoms, and the relative stereochemistry of the substituents on the phosphine sites. X-ray data were collected on a Syntex $P2_1$ autodiffractometer at −110 °C, and structures were refined by the full-matrix least-squares method. For *c*-PSPS·Ni: a = 15.882 (5) Å, b = 16.865 (5) Å, c = 12.713 (1) Å, β = 97.35 (2)°, monoclinic, $P2_1/c$, Z = 4, R = 0.041, R_w = 0.039 for 6335 reflections with $F_o \geq 4\sigma(F_o)$. For *c*-P_3S·Pt: a = 13.359 (4) Å, b = 15.308 (3) Å, c = 20.271 (6) Å, β = 109.31 (2)°, monoclinic, $P2_1/c$, Z = 4, R = 0.052, R_w = 0.047 for 6954 reflections with $F_o \geq 4\sigma(F_o)$. For *t*-P_3S·NiCl: a = 12.449 (3) Å, b = 21.574 (4) Å, c = 14.002 (9) Å, β = 97.82 (4)°, monoclinic, $P2_1/c$, Z = 4, R = 0.063, R_w = 0.051 for 5116 reflections with $F_o \geq 4\sigma(F_o)$. For *t*-P_3S·Ni(MeCN): a = 14.909 (6) Å, b = 23.737 (5) Å, c = 11.238 (2) Å, β = 100.07 (3)°, monoclinic, $P2_1/c$, Z = 4, R = 0.043, R_w = 0.039 for 6706 reflections with $F_o \geq 4\sigma(F_o)$. Revised structural parameters for *c*-PSPS·Pt based on refinement with a corrected absorption factor are also reported.

While a considerable amount of effort has been directed toward the synthesis of polyphosphino macrocycles (MC),[2-9] relatively little is known about how the nature of the ligand affects the properties of a coordinated transition metal (TM). Fundamental questions of how ring size, various combinations of donor atoms, the geometrical arrangement of donor atoms, the types of substituents on the donor atoms, and the relative stereochemistries within the MC can modify the properties of a TM remain to be probed. To answer these questions, the MC must be systematically modified by changing only one variable at a time followed by coordination with a variety of TM. This is a formidable challenge when the number of ligand variables and the number of transition metals are considered.

The effect of the relative configuration at the *trans*-phosphino site within the MC on TM coordination has been studied by Ciampolini and co-workers using the five isomers of the 18-P_4O_2 ligand (**1**).[8] A combination of X-ray crystallography and UV–vis spectroscopy on Ni(II) and Co(II) complexes of **1** was used to demonstrate that these MC could be hexa-, penta-, or tetradentate depending on the relative configurations at the phosphino sites. While the synthesis and analysis of the coordination chemistry of these 18-P_4X_2 macrocycles required substantial effort, this study clearly demonstrated that the relative configurations at the phosphine sites force the macrocyclic backbone to adopt particular conformations that result in either placing X in or out of bonding distance to the TM.

Our group has investigated the effect of exchange of a heteroatom X for a phosphine site in the 11-P_3 (→11-P_2X) (**2**) system.[1,10] These MC were found to act as bidentate and tri-

(1) Phosphinomacrocycles. 16. For part 15 see: Kyba, E. P.; Davis, R. E.; Liu, S.-T.; Hassett, K. A.; Larson, S. B. *Inorg. Chem.* **1985**, *24*, 4629.
(2) (a) Horner, L.; Kunz, H.; Walach, P. *Phosphorus Relat. Group V Elem.* **1975**, *6*, 63. (b) Horner, L.; Kunz, H.; Walach, P. *Phosphorus Sulfur* **1978**, *5*, 171.
(3) Rosen, W.; DelDonno, T. A. *J. Am. Chem. Soc.* **1977**, *99*, 8051.
(4) (a) Kyba, E. P.; Hudson, C. W.; McPhaul, M. J.; John, A. M. *J. Am. Chem. Soc.* **1977**, *99*, 8053. (b) Kyba, E. P.; Davis, R. E.; Hudson, C. W.; John, A. M.; Brown, S. B.; McPhaul, M. J.; Liu, L.-K.; Glover, A. C. *J. Am. Chem. Soc.* **1981**, *103*, 3868. (c) Kyba, E. P.; Chou, S.-S. P. *J. Org. Chem.* **1981**, *41*, 860. (d) Kyba, E. P.; Heumüller, H. H. *ACS Symp. Ser.* **1981**, 473. (e) Kyba, E. P.; Liu, S.-T. *Inorg. Chem.* **1985**, *24*, 1613. (f) Kyba, E. P.; John, A. M.; Brown, S. B.; Hudson, C. W.; McPhaul, M. J.; Harding, A.; Larson, K.; Niedzwiecki, S.; Davis, R. E. *J. Am. Chem. Soc.* **1980**, *102*, 139. (g) Kyba, E. P.; Clubb, C. N.; Larson, S. B.; Schueler, V. J.; Davis, R. E. *J. Am. Chem. Soc.* **1985**, *107*, 2141.
(5) (a) Stelzer, O.; Bartsch, R.; Hietkamp, S.; Morton, S.; Peters, H. *Inorg. Chem.* **1983**, *22*, 3624. (b) Stelzer, O.; Bartsch, R.; Heitkamp, S.; Peters, H. *Inorg. Chem.* **1984**, *23*, 3304.
(6) Norman, A. D.; Diel, B. N.; Haltiwanger, R. C. *J. Am. Chem. Soc.* **1982**, *104*, 4700.
(7) Scanlon, L. G.; Tsao, Y.-Y.; Toman, K.; Cummings, S. C.; Meek, D. W. *Inorg. Chem.* **1982**, *21*, 1215.
(8) (a) Ciampolini, M.; Dapporto, P.; Nicoletta, N.; Zanobini, F. *Inorg. Chem.* **1983**, *22*, 13. (b) Ciampolini, M.; Dapporto, P.; Die, A.; Nardi, N.; Zanobini, F. *Inorg. Chem.* **1982**, *21*, 489. (c) Ciampolini, M.; Dapporto, P.; Nardi, N.; Zanobini, F. *J. Chem. Soc., Chem. Commun.* **1980**, 177. (d) Ciampolini, M.; Dapporto, P.; Innocenti, P.; Nardi, N.; Zanobini, F. *Chem. Abstr.* **1984**, *100*, 156700x. (e) Ciampolini, M.; Dapporto, P.; Nardi, N.; Zanobini, F. *Inorg. Chim. Acta* **1980**, *45*, L239. (f) Ciampolini, M.; Nardi, N.; Zanobini, F. *Inorg. Chim. Acta* **1983**, *76*, L17.
(9) Ansell, C. W. G.; Cooper, M. K.; Dancey, K. P.; Duckworth, P. A.; Henrick, K.; McPartlin, M.; Tasker, P. A. *J. Chem. Soc., Chem. Commun.* **1986**, 439.
(10) (a) Kyba, E. P.; Campbell, K. A.; Fox, M. A. *Inorg. Chem.* **1981**, *20*, 4163. (b) Kyba, E. P.; Alexander, D. C.; Höhn, A. *Organometallics* **1982**, *1*, 1619. (c) Kyba, E. P.; Brown, S. B. *Inorg. Chem.* **1980**, *19*, 2159. (d) Davis, R. E.; Kyba, E. P.; John, A. M.; Yep, J. M. *Inorg. Chem.* **1980**, *19*, 2540. (e) The periodic group notation in parentheses is in accord with recent actions by IUPAC and ACS nomenclature committees. A and B notation is eliminated because of wide confusion. Groups IA and IIA become groups 1 and 2. The d-transition elements comprise groups 3 through 12, and the p-block elements comprise groups 13 through 18. (Note that the former Roman number designation is preserved in the last digit of the new numbering: e.g., III → 3 and 13.)

0020-1669/87/1326-1647$01.50/0

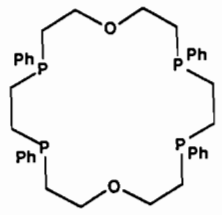

1

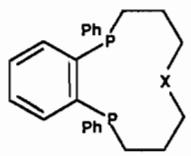

2
a, X = PPh
b, X = S
c, X = NMe

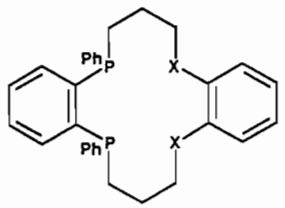

3
a, X = PPh
b, X = AsMe
c, X = S
d, X = NMe
e, X = O

dentate ligands with group VI (group 6[10e]) metal carbonyls[10a,c] and with cobalt(II) halides,[10b] depending upon the unique heteroatom and upon the stoichiometry of reagents. The oxidation potentials for the *fac*-tricarbonylmolybdenum complexes of **2a–c** were found to vary by 0.47 V with the **2a** complex being the least easily oxidized and the **2c** complex being the most easily oxidized.[10a]

While several 14-P_2X_2 macrocycles **3a–d** have been synthesized,[4a–c] little complexation behavior has been reported,[10b,11] primarily because the complexes tended to be amorphous powders, which made characterization difficult. In the few complexes that were characterized, the macrocycles acted as bidentate phosphine ligands; i.e., the intramolecular "modifying heteroatoms" X did not compete with intermolecular phosphines. Thus, the reaction of **3e** with $CoCl_2$ resulted in a complex with a ligand to metal ratio of 2:1, $(\mathbf{3e})_2CoCl_2$.[10b] The sulfur analogue, **3c**, gave a similar 2:1 complex with iron(II) chloride, shown schematically as **4**, which was characterized by an X-ray crystal structure determination.[12]

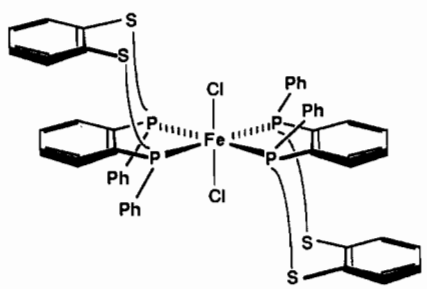

4

On the basis of the examination of X-ray structures of TM complexes that involve the 1,2-diphosphinobenzo moiety, we felt that if a 1-X-2-phosphinobenzo moiety were incorporated into the macrocyclic ligand, it would be highly likely that X would indeed be involved in the coordination of a TM. In this regard, we have recently reported the high-dilution syntheses of such macrocycles with X = S (**5–7**) and an X-ray crystal structure determination of a Pt(II) complex that demonstrated the viability of such an approach.

Ligands **5** and **6** are structural isomers of **3c**, and each exists as a pair of diastereomers (**C** and **T**) where the phenyl substituents on phosphorus are either cis or trans, respectively. For the sake of convenience, **5C,T** and **6C,T** will be referred to as *c*- and *t*-PSPS and *c*- and *t*-PSSP, respectively. Species **7** also was obtained only

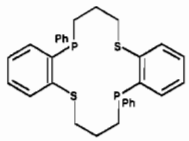

5C,T

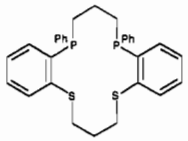

6C,T

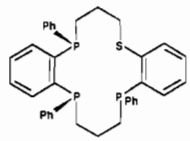

7C,T

as the two isomers shown, and we shall refer to them as *c*- and *t*-P_3S. We have rationalized the absence of the third possible diastereomer (phenyl groups trans across the *o*-phenylene link).[4b] Finally, we shall refer to *cis,cis,cis*-**3a** as *c*-P_4 and *cis*-**3c** as *c*-P_2S_2.

With these ligands, the effects of heteroatom placement, stereochemistry at phosphorus, and the ratio of phosphorus to sulfur within a macrocyclic ligand upon the properties of a coordinated TM were studied and are reported herein.

Results and Discussion

Synthesis of the Ni(II) Triad Complexes. A series of complexes of the 14-P_nS_{4-n} cyclic ligands and the nickel(II) triad was prepared in yields after recrystallization in the 18–76% range (Table I). A few complexes were not crystallized but gave satisfactory combustion analyses—these were obtained generally in higher yields (89–94%).

The nickel(II) dichloride complexes were prepared by adding a THF solution of the MC to a THF/EtOH (2:1, v/v) solution of nickel chloride hexahydrate. The resulting complexes were quite soluble in the reaction medium and required the addition of a nonpolar solvent such as diethyl ether and cooling to −20 °C to effect precipitation. The resulting materials were amorphous powders that were recrystallized from $MeCN/CH_2Cl_2$ containing a small amount of ethanol. The nickel(II) perchlorate complexes were prepared by simply mixing equimolar amounts of the MC and nickel(II) perchlorate hexahydrate in THF. This resulted in precipitation of the complex, which was filtered and recrystallized. The nickel(II) chloride perchlorate complexes were prepared by mixing the macrocycle with "$NiCl(ClO_4)$" generated in situ from $NiCl_2(H_2O)_6$ and $Ni(ClO_4)_2(H_2O)_6$.[13] This technique worked well in some cases and poorly in others, where inseparable mixtures of MC·$NiCl(ClO_4)$ and MC·$Ni(ClO_4)_2$ were obtained, e.g., with MC = *c*-PSSP and *c*-P_3S. The mixtures were indicated by elemental analyses and molar conductivities that were much too high for the expected $[MC{\cdot}NiCl][ClO_4]$ 1:1 electrolyte. The palladium and platinum compounds were prepared by using $(COD)PdCl_2$ or $(COD)PtCl_2$ (COD = 1,5-cyclooctadiene), respectively, followed by anion metathesis with the appropriate noncoordinating anion and recrystallization from acetonitrile.

Table I summarizes the yields, colors, solvents used for recrystallization, combustion analyses, and selected physical properties of the 22 macrocycle–TM complexes prepared in this work.

Structures of TM Complexes. The structures of four MC–TM complexes ($[c\text{-PSPS·Ni}][ClO_4]_2{\cdot}CH_3CN$, $[c\text{-}P_3S{\cdot}Pt][PF_6]_2$, $[t\text{-}P_3S{\cdot}Ni(NCMe)][ClO_4]_2$, and $[t\text{-}P_3S{\cdot}NiCl][ClO_4]{\cdot}CH_2Cl_2$) were determined and the results are presented as ORTEP plots, along with that determined previously for $[c\text{-PSPS·Pt}][PF_6]_2{\cdot}C_6H_6$ (Figure 1). Even a casual inspection of these structures reveals that the three complexes derived from the *c*-MC are quite different from the two obtained from the *t*-MC. The former are essentially square planar tetracoordinate, while the latter are pentacoordinate and much less symmetrical.

The heavy-atom cores of the three *c*-MC complexes are nearly but not rigorously square planar; the metal center is somewhat out of the plane defined by the four ligating sites on the side of the phenyl substituents, and the L^1–M–L^2 bond angles are close to but not equal to 90° (Table II). The M–P and M–S bond lengths are essentially indistinguishable, and the Ni–P (or S) bond lengths are about 0.11 (±0.02) Å shorter than the corresponding Pt–P (or S) bond lengths (Table II). In contrast to the three *c*-MC complexes, the two *t*-MC complexes exhibit a geometry that is approximately trigonal bipyramidal (tbp, *t*-P_3S·NiCl) and a ge-

(11) Hudson, C. W. Ph.D. Dissertation, University of Texas at Austin, 1977.
(12) Kyba, E. P.; Davis, R. E., unpublished results.
(13) Meek, D. W.; DuBois, T. D. *Inorg. Chem.* **1969**, *8*, 146 and references therein.

Table I. Yields, Physical Properties, and Related Data for $[MC-TM](X)_2$[a]

complex	yield, %	color	recryst solv[c]	combustion analysis[d] % C found (calcd)	combustion analysis[d] % H found (calcd)	molar cond[e]	UV–vis λ_{max} (ϵ)[f]	^{31}P NMR δ (Δ; J Hz)[f,g]
c-PSPS·$NiCl_2(H_2O)_2$	73	yellow	MeCN/CH_2Cl_2/MeOH	51.42 (51.45)	5.06 (4.80)	122	266 (1.12 × 10^4), 306 (9075)	50.2 (br)
t-P_3S·$NiCl_2(H_2O)_2$	82	gr-black	MeCN/CH_2Cl_2/MeOH	56.49 (57.02)	5.40 (5.18)	113	310 (1.40 × 10^4), 478 (1014)	60.0 (84.1; dd, J = 72, 49), 26.9 (53.9; dd, J = 260, 49), 20.5 (44.6; dd, J = 260, 72)
c-P_3S·$NiCl_2(H_2O)_3$	60	rust	—	55.85 (55.70)	5.77 (5.32)	124	292 (1.29 × 10^4), 402 (571)	50.0 (complex m)
(*t*-PSSP·NiCl)(ClO_4)	37	purple	EtOH/CH_2Cl_2	50.44 (50.76)	4.25 (4.26)	127	554 (1140), 728 (710)	*h*
(*c*-PSPS·NiCl)(ClO_4)	49	caramel	MeCN	50.49 (50.76)	4.45 (4.26)	127	430 (530)	43.5 (65.9)
(*t*-PSPS·NiCl)(ClO_4)	84	rust	—	50.49 (50.76)	4.28 (4.26)	132	448 (1140)	50.4 (76.4)[i]
(*t*-P_3S·NiCl)(ClO_4)(CH_2Cl_2)[b]	46	dk green	EtOH/CH_2Cl_2	51.32 (51.01)	4.37 (4.16)	134	473 (1080), 626 (603)	60.6 (89.1; dd, J = 73, 45), 27.7 (56.2; dd, J = 256, 45) 16.6 (45.1; dd, J = 256, 73)
(*c*-PSSP-Ni)(ClO_4)$_2$(C_6H_6)[b]	53	orange	MeCN/C_6H_6	50.94 (50.73)	4.35 (4.26)	329	422 (820)	41.3 (66.3)
(*t*-PSSP-Ni)(ClO_4)$_2$	94	mustard	—	46.40 (46.54)	4.17 (3.91)		415 (830), 543 (830)	38.7 (66.3; d, J = 95), 23.8 (51.4; *d*, J = 95)[j]
(*c*-PSPS-Ni)(ClO_4)$_2$	76	orange	MeCN	46.61 (46.54)	4.00 (3.91)	326	420 (770)	43.4 (65.8)
(*t*-PSPS-Ni)(ClO_4)$_2$	57	yellow	MeCN	46.46 (46.54)	4.12 (3.91)		405 (970)	52.3 (78.3)
(*c*-P_3S·Ni)(ClO_4)$_2$	41	orange	MeCN	50.62 (50.85)	4.21 (4.15)	308	392 (1020)	50.5 (75.5; dd, J = 190, 36), 49.5 (74.5; dd, J = −85, 36) 42.0 (67.0; dd, J = 190, −85)[k]
(*t*-P_3S·Ni)(ClO_4)$_2$(MeCN)[b]	44	red	MeCN	51.08 (51.15)	4.37 (4.29)	332	407 (1550)	57.7 (86.2; dd, J = 73, 48), 38.9 (67.4; dd, J = 230, 73), 28.8 (57.3; dd, J = 230, 48)
(*c*-P_4·Ni)(ClO_4)$_2$	41	yellow	MeCN	54.43 (54.46)	4.00 (4.35)		376 (2970)	50.5 (76.6)
(*c*-PSSP·Pd)(PF_6)$_2$	37	white	Me_2CO	39.52 (39.47)	3.33 (3.31)	336	291 (1.49 × 10^4)	39.9 (64.9)
(*c*-PSSP·Pd)(BPh_4)$_2$	53	yellow	MeCN	74.03 (74.29)	5.72 (5.59)			48.4 (70.8)
(*c*-P_3S·Pd)(PF_6)$_2$(MeCN)$_3$[b]	47	yellow	MeCN	45.49 (45.36)	3.89 (3.99)		270 (2.53 × 10^4)	48.7 (75.7; dd, J = 27, 11), 45.2 (58.3; dd, J = 306, 27)
(*c*-PSSP·Pt)(ClO_4)$_2$	23	white	MeCN	39.88 (39.75)	3.33 (3.32)	325	271 (sh, 8.46 × 10^3)	28.2 (53.2; J = 2729)[m]
(*c*-PSPS·Pt)(PF_6)$_2$	18	white	MeCN/C_6H_6	35.81 (35.97)	3.20 (3.02)	352	296 (1.71 × 10^4) 234 (sh, 4.23 × 10^4)	39.4 (61.8; J = 2148)
(*c*-P_3S·Pt)(PF_6)$_2$	35	white	MeCN	40.34 (40.08)	3.24 (3.27)			39.4 (64.4; d, J = 16, 2165), 38.9 (63.9; d, J = 18, 2132), 32.9 (32.9; dd, J = 18, 16, 2727)
(*t*-P_3S·Pt)(BPh_4)$_2$	50	white	MeCN	70.72 (70.74)	5.44 (5.30)	229	272 (1.51 × 10^5)	49.3 (77.8; dd, J = 285, 20, 2322), 34.9 (63.4; dd, J = 285, 10, 2219), 30.0 (58.5; dd, J = 20, 10, 2615)
(*c*-P_2S_2·Pt)(PF_6)$_2$	33	white	MeCN	35.81 (35.97)	3.02 (3.02)			36.2 (63.2; J = 2801)

[a] See text for definitions of the abbreviations of the complex names. [b] Presence of solvent was confirmed by ^{1}H NMR spectroscopy. [c] A dash means that the complex was not recrystallized. [d] Analyses carried out by Galbraith Labortories, Knoxville, TN. [e] Measured on ca. 0.5 × 10^{-3} M acetonitrile solutions; units $cm^2\ \Omega^{-1}\ mol^{-1}$. [f] Determined in acetonitrile solutions. Unless otherwise noted, the absorptions given are singlets. [g] Δ = coordination chemical shift in ppm. [h] Unable to detect absorptions at 25 °C or −42 °C. [i] Spectrum at −42 °C consists of two broad singlets at 58 and 44 ppm. [j] Spectrum taken at −42 °C. No spectrum was observable at 25 °C. [k] Second-order spectrum matched by computer simulation with parameters given. [m] The large coupling constant is that due to ^{31}P–^{195}Pt.

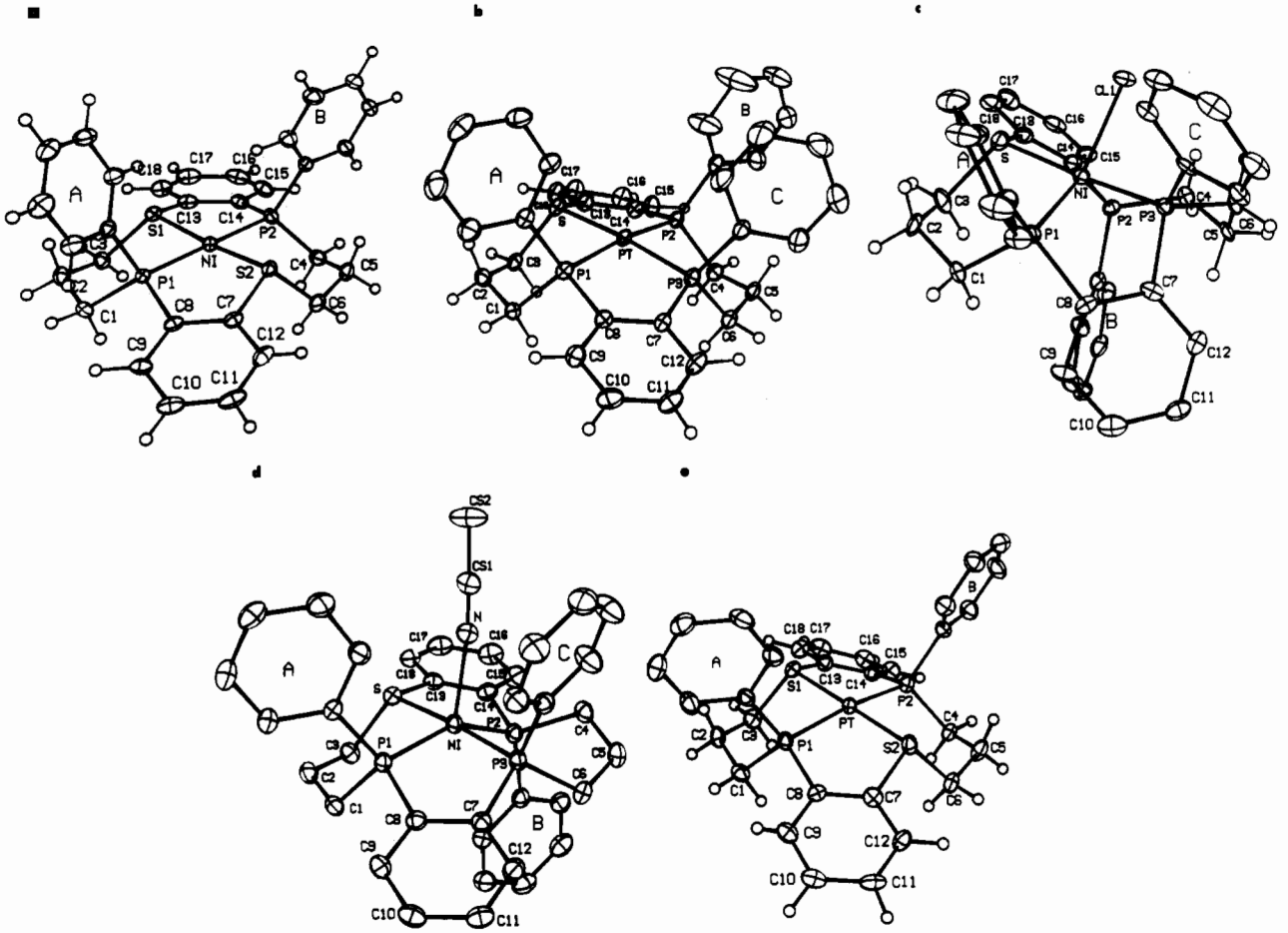

Figure 1. ORTEP plots with non-hydrogen atoms represented as 35% equiprobability ellipsoids: (a) *c*-PSPS·Ni^{II}; (b) *c*-P_3S·Pt^{II}; (c) *t*-P_3S·$Ni^{II}Cl$; (d) *t*-P_3S·Ni^{II}(NCMe); (e) *c*-PSPS·Pt^{II} (revised data).

Table II. Bond Lengths (Å) and Angles (deg) of the Heavy-Atom Cores of Ni(II) and Pt(II) Complexes of Ligands **5C**, **7C**, and **7T**[a]

	c-PSPS· Pt	*c*-PSPS· Ni	*c*-P_3S· Pt	*t*-P_3S· NiCl	*t*-P_3S· Ni(MeCN)
P1–M	2.300	2.189	2.289	2.171	2.184
P2–M	2.293	2.179	2.283	2.227	2.181
P3(S2)–M	2.285	2.172	2.255	2.139	2.157
S(1)–M	2.294	2.158	2.317	2.200	2.211
P1–M–S(1)	91.9	91.3	92.0	96.2	91.1
P1–M–P3(S2)	87.5	88.4	87.4	84.0	87.1
P1–M–P2	170.7	179.6	171.5	126.8	149.6
S(1)–M–P2	87.3	88.7	87.8	89.4	89.2
S(1)–M–P3(S2)	179.3	173.8	174.5	175.5	175.9
P2–M–P3(S2)	93.3	91.5	92.0	94.1	90.5
X–M–P1[b]				138.8	112.4
X–M–P2[b]				94.0	98.0
X–M–S(1)[b]				88.2	85.6
X–M–P3(S2)[b]				88.6	98.5

[a] The uncertainties in the bond lengths are ≤|0.002|. The uncertainties in the bond angles are ≤|0.1|. Complete tables of bond lengths and angles are given in the supplementary material. [b] X = Cl or MeCN in the *t*-P_3S complexes.

ometry that is between tbp and square pyramidal [sp, *t*-P_3S·Ni(NCMe)].

The fundamental differences in the core geometries among the metal complexes of the *c*- and *t*-MC can be attributed primarily to the dihedral angles in the six-membered chelates imposed by the relative configurations of the phosphine ligands. Examination of these dihedral angles (Table III, entries 1–6 and 7–12) for the *c*-MC complexes reveals nicely alternating +gauche/−gauche angles typical of a chairlike six-membered ring. It is not surprising that there are deviations from the ideal 60° torsional angles, considering that bond lengths vary by as much as 50% within each ring (e.g., C–C vs. P–M). With the *t*-MC complexes, the rings that involve P1 and S are chairlike, although slightly flattened relative to the *c*-MC–TM species (Table III, entries 1–6, last two columns). In contrast, *t*-P_3S·Ni(NCMe) exhibits a twist-boat conformation for the six-membered ring Ni–P2–C4–C5–C6–S (Table III, entries 7–12, last column). A flattened chair conformation opposite to those observed for all of the others is present for the same ring in *t*-P_3S·NiCl (Table III, entries 7–12, next to last column). These observations may be rationalized by considering **8** and **9**, which show the effect of having phenyl groups

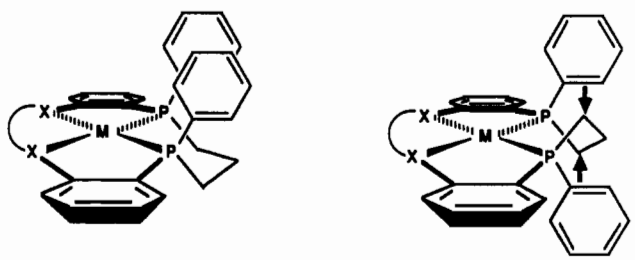

8 **9**

on phosphorus trans across a trimethylene chain in a MC–TM complex. When the phenyl groups are cis, as in **8**, a comfortable chair conformation is achievable while nearly square-planar geometry is still maintained about the metal. In contrast, when the phenyl groups are trans, as in **9**, then the two CH_2 moieties attached to the two phosphorus atoms are mutually above and below the plane defined by PMP. In order to join these two CH_2 groups with the third CH_2, a substantial torque is developed that tends to distort the geometry about the metal away from square planarity. In the case of *t*-P_3S·NiCl, a chair of opposite cant for this ring is obtained along with tbp geometry about the metal.

Presumably the enforced distortion from square planarity by the *t*-MC enhances the tendency toward pentacoordinate geometry.

Table III. Dihedral Angles within the Six- and Five-Membered Chelates in the Ni(II) and Pt(II) Complexes (deg) of Ligands **5C**, **7C**, and **7T**[a]

		c-PSPS·Pt(II)[b]	*c*-PSPS·Ni(II)[c]	*c*-P_3S·Pt(II)[d]	*t*-P_3S·Ni(II)Cl[e]	*t*-P_3S·Ni(II)(MeCN)[e]
1	M-P1-C1-C2	−60.6	−56.7	−59.9	−51.4	−58.6
2	P1-C1-C2-C3	71.0	66.7	70.4	69.0	67.4
3	C1-C2-C3-X	−78.1	−74.3	−78.2	−76.1	−71.1
4	C2-C3-X-M	70.4	70.2	70.5	64.4	68.3
5	C3-X-M-P1	−52.4	−52.4	−52.9	−42.5	−53.2
6	X-M-P1-C1	50.5	47.9	50.5	36.9	47.7
7	M-P2-C4-C5	−57.4	−62.0	−61.0	60.2	74.6
8	P2-C4-C5-C6	72.6	69.0	69.4	−73.1	−30.1
9	C4-C5-C6-Y	−78.1	−71.9	−70.0	68.2	−34.3
10	C5-C6-Y-M	63.9	65.2	61.2	−49.5	56.0
11	C6-Y-M-P2	−44.0	−50.3	−45.0	32.0	−10.7
12	Y-M-P2-C4	43.2	50.6	45.4	−37.6	−43.0
13	M-P1-C8-C7	7.7	16.2	5.2	24.0	8.6
14	P1-C8-C7-Y	8.4	1.6	3.3	5.8	7.1
15	C8-C7-Y-M	−20.0	−18.7	−10.2	−33.8	−19.9
16	C7-Y-M-P1	18.3	22.1	10.0	37.9	19.3
17	Y-M-P1-C8	−15.2	−21.6	−8.7	−34.9	−16.1
18	M-X-C13-C14	−6.5	−14.7	−7.5	14.2	5.1
19	X-C13-C14-P2	−9.6	2.6	−4.2	4.4	12.4
20	C13-C14-P2-M	20.5	10.7	13.7	−20.5	−23.8
21	C14-P2-M-X	−18.5	−15.3	−13.7	22.7	20.7
22	P2-M-X-C13	14.5	16.4	12.0	−20.8	−15.6

[a] The uncertainty in the values does not exceed |0.1|. [b] M = Pt; X = S1; Y = S2. [c] M = Ni; X = S1, Y = S2. [d] M = Pt; X = S; Y = P3. [e] M = Ni; X = S; Y = P3.

Thus [*c*-PSPS·Ni][$(ClO_4)_2$] did not coordinate acetonitrile from which it was recrystallized but [*t*-P_3S·Ni][$(ClO_4)_2$] did (see Figure 1). As expected, when an anionic ligand (e.g., Cl^-, as in $(Cl)_2$ and $(Cl)(ClO_4)$ complexes) was available, it gave pentacoordinate complexes, as indicated by molar conductivities in acetonitrile in the range of 120 Ω^{-1} cm^2 mol^{-1} (Table I), which are expected for 1:1 electrolytes.[14] Presumably, these are square pyramidal with the chloride in the apical position, although we have no structural example of this case as yet. With the *t*-MC, there is a strong tendency toward pentacoordinate geometry where the fifth coordination site is occupied by either chloride ion or, in its absence, acetonitrile, the solvent we found to be the best from which to crystallize and recrystallize these complexes.

A question that must be addressed is whether or not the thioether sites remain coordinated in solution. A study of molecular models of TM complexes of *c*- and *t*-PSSP, *c*- and *t*-PSPS, and *c*- and *t*-P_3S indicates that in all cases the mono- or dithiodecoordinated species are relatively comfortable from the standpoint of the conformations of the decoordinated strands. In addition, there is sufficient room to replace the decoordinated sulfur site with an acetonitrile ligand. One probe to examine this is the ^{31}P NMR spectrum of each complex. It is well-known that chelating phosphines in a five-membered ring are especially deshielded in the ^{31}P NMR spectrum (ca. 25–35 ppm), whereas those in a six-membered ring are shielded (ca. 5–15 ppm), relative to nonchelating congeners.[15] A relevant example is that of **10**, which

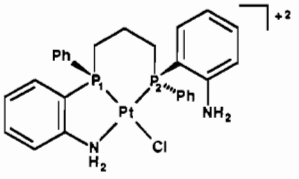

10

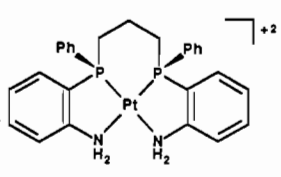

11

has both ring sizes.[16] The coordination chemical shift Δ of P_1 is 46 ppm, whereas that of P_2 is 15 ppm. These values reflect the extra deshielding of the five-membered chelate (somewhat attenuated by the six-membered chelate effect) on P_1 and the extra shielding effect of a six-membered chelate on P_2. When the second phosphino site is also incorporated into a five-membered chelate (**11**), only the large Δ (46 ppm) is observed.

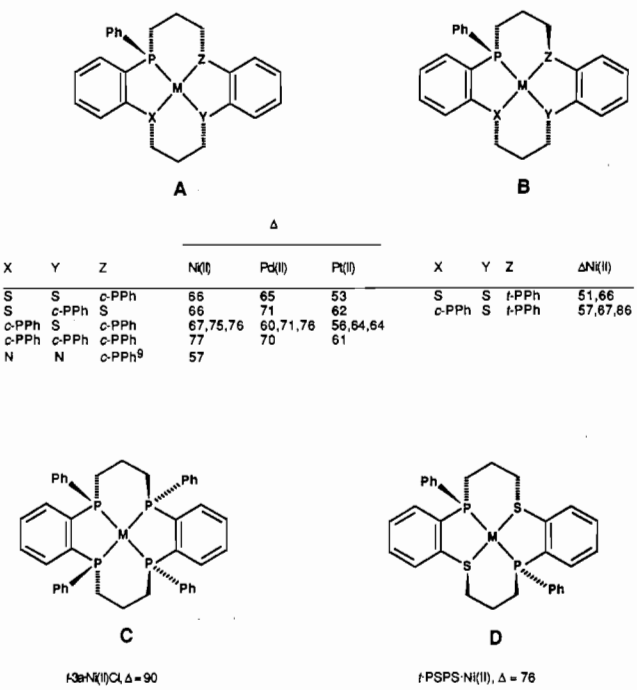

Figure 2. ^{31}P coordination chemical shifts (Δ, ppm) of several MC–TM complexes, extracted from Table I.

Figure 2 presents the ^{31}P coordination chemical shifts of the complexes as a function of stereochemistry of the heteroatoms. It is clear from the magnitude of these values that the phosphine ortho to the thioether site is substantially deshielded, although less than one ortho to a phosphino site. We have shown, however, that Δ for the open-chain model for these PS MC, i.e., **12**, is about 6 ppm less than that for the corresponding diphosphine.[17] The fact that the thioether site was bound to the metal center in solution was established by the observation of a substantial ^1H

(14) Geary, W. J. *Coord. Chem. Rev.* **1971**, *7*, 81.
(15) Garrou, P. E. *Chem. Rev.* **1981**, *81*, 229.
(16) Ansell, C. W. G.; Cooper, M. K.; Dancey, K. P.; Duckworth, P. A.; Henrick, K.; McPartlin, M.; Organ, G.; Tasker, P. A. *J. Chem. Soc., Chem. Commun.* **1985**, 437.
(17) Liu, S.-T.; Kyba, E. P., unpublished results.

Scheme I

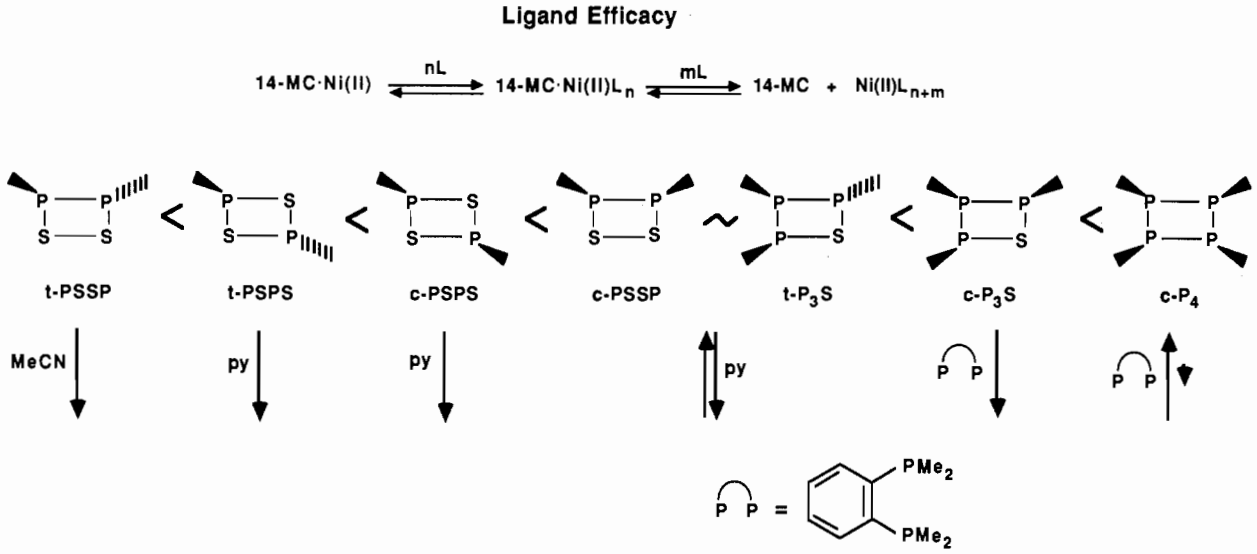

coordination chemical shift of the protons on the carbon atom attached to sulfur in the case of the Ni(II) complex. With the platinum complexes additional data, $^{195}Pt-^{31}P$ coupling constants, can be used to probe this coordination question. Bennett and Appleton have shown that the acetonitrile ligand trans to a phosphine will cause a larger $^1J_{Pt-P}$ than will a chloride ion.[18] Although there appear to be no reports of the trans effect of thioethers on $^1J_{Pt-P}$, it is known that trans thiolates cause such coupling to be ca. 0.8 of those caused by *trans*-Cl.[18] In addition, it is known that the $^1J_{Pt-P}$ for a *trans*-NRR′ is ca. 0.95 of that due to a *trans*-NHRR′.[16] In complex **10**, which is an excellent model for our complexes, $^1J_{Pt-P}$ = 3269 Hz for the phosphine trans to the chloride. On the basis of the above considerations, it might be expected that a phosphine in **10** trans to acetonitrile would have a Pt–P coupling constant >3269 Hz. One would predict also that $^1J_{Pt-P}$(trans to S) ~ 0.8(3269) ~ 2620 Hz in our complexes. The observed values are in the range 2615–2729 Hz (Table I). Bennett and Appleton[18] have also shown that $^1J_{Pt-P}$(trans to P) ~ 0.65 of that of Cl, leading to the prediction that such coupling constants in our complexes would be about 0.65(3269) ~ 2120 Hz. We observe these coupling constants to be in the range of 2132–2322 Hz (Table I). Thus, the $^{195}Pt-^{31}P$ coupling constant data shown in Table I are all in accord with the thioether sites being bound in solution just as we have found them to be in the solid state.

Coordinating Ability of the MC. In order to determine at least qualitatively the relative ability of the seven MC in this study to coordinate a TM center, a series of competitive decomplexations on the nickel(II) perchlorate complexes were carried out. The results are summarized in Scheme I. A range of coordinating ability is spanned from one that is not competitive with acetonitrile to one that is displaced only to a small extent by an excess of the excellent ligand 1,2-phenylenebis(dimethylphosphine).[19] The displacements require on the order of minutes to hours to occur, and there is no indication of rapid exchange when both the free and complexed MC are observable by ^{31}P NMR spectroscopy. Presumably this is also indicative of the fact that the thioether sites are bound to the metal in solution (vide supra). In accord with this is the observation that the pentacoordinate [*t*-PSSP·NiCl][ClO_4] is essentially stable in acetonitrile, whereas, with the corresponding diperchlorate salt, the MC is displaced by the solvent over several hours. It is well-known that such displacements proceed via an associative mechanism.[20] Since the pentacoordinate complex is coordinatively saturated (if the thioether sites are bound), the rate of MC displacement by solvent is greatly reduced.

Not surprisingly, the ligating ability increases with increasing numbers of phosphine sites. Within the P_2S_2 MC, the worst ligand is *t*-PSSP, which has the configuration depicted as B in Figure 2. We have commented above on the consequences of having a *trans*-Ph_2 arrangement across the six-membered chelate (structures **8** and **9**). The *t*-PSPS complex (D, Figure 2) does not have trimethylene units spanning trans positions in a six-membered chelate and does not allow the saddlelike arrangement of the MC around the metal, as shown for the *c*-MC complexes in Figure 1. Examination of Dreiding models of A (Figure 2) indicates that the latter is more strained. Both *c*-PSPS and *c*-PSSP have the saddle-type of conformation (A, Figure 2). Presumably, the reason that the latter is a better ligand is that it has the two phosphino moieties as a six-membered chelate, whereas the former does not. The *t*-P_3S (type B, Figure 2) is approximately equivalent to *c*-PSSP as a ligand, indicating how destabilizing it is to have the $(CH_2)_3$ moiety spanning trans positions, as shown in **9**. Finally, comparison of *c*-P_3S and *c*-P_4 indicates the strong effect of replacing one PPh with an S unit. Calculation of the equilibrium constants for decomplexation of these two species (see Experimental Section) indicates that *c*-P_4 is ca. 10^3 times a better ligand than *c*-P_3S toward Ni^{2+} in acetonitrile.

Electrochemistry of the MC–TM Complexes. The electrochemistry of monodentate and bidentate phosphine complexes of Ni(II),[21] as well as Pd(II) and Pt(II),[21a,b] has been studied. The ease of reduction decreased in progressing from the first row to the third row. With monodentate phosphines, the bulkiness of the ligand, the π-acceptor ability, and the presence of added halide ions strongly affected the electrochemistry of the Ni(II) triad.[21b] If the phosphine ligands were small (PEt_3, PEt_2Ph) or chelating ($Ph_2PCH_2CH_2PPh_2$, dppe), then good evidence was presented for two separate one-electron reductions starting with the Ni(II) complex, illustrated as follows for the square-planar dppe complex (**12**).[21a,d] The odd-electron complex **13** has been suggested to

$$[(dppe)_2Ni(II)]^{+2} \underset{-e^-}{\overset{+e^-}{\rightleftharpoons}} [(dppe)_2Ni(I)]^{+} \underset{-e^-}{\overset{+e^-}{\rightleftharpoons}} (dppe)_2Ni(0)$$

12 **13** **14**

have a distorted tetrahedral structure,[21a] and of course **14** is tetrahedral.[22] With phosphines that did not give stable $[Ni^{II}L_4]^{2+}$ species so that ligand-exchange processes took place prior to and following the electrochemical steps, more complex behavior was

(18) Appleton, T. G.; Bennett, M. A. *Inorg. Chem.* **1978**, *17*, 738.
(19) Kyba, E. P.; Liu, S.-T.; Harris, R. L. *Organometallics* **1983**, *2*, 1877.
(20) Cotton, F. A.; Wilkinson, G. *Advanced Inorganic Chemistry*, 4th ed.; Wiley: New York, 1980; pp 1198–1202.
(21) (a) Martelli, M.; Pilloni, G.; Zotti, G.; Daolio, S. *Inorg. Chim. Acta* **1974**, *11*, 155. (b) Warren, L. F.; Bennett, M. A. *Inorg. Chem.* **1976**, *15*, 3126. (c) Bontempelli, G.; Magno, F.; Nobili, M. D.; Schiavon, G. *J. Chem. Soc., Dalton Trans.* **1980**, 2288. (d) Bontempelli, G.; Magno, F.; Schiavon, G.; Corain, B. *Inorg. Chem.* **1981**, *20*, 2579.
(22) Chatt, J.; Hart, F. A.; Watson, H. R. *J. Chem. Soc.* **1962**, 2537.

observed and in many cases the analogues of **13** were not observable, facile disproportionation reactions intervening instead.[21d] It is thus curious that, with 1,2-phenylenebis(dimethylphosphine) in place of dppe in **12**, only a two-electron reduction process was reported. Before considering our electrochemical results, it is instructive to consider what geometries are attainable by our MC about the metal center. As illustrated in Figure 1, square-planar, square-pyramidal, and trigonal-bipyramidal geometries have been observed, the latter two with *t*-MC. Inspection of structure **15**,

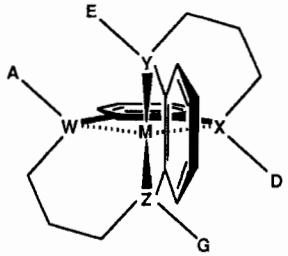

15

which is a drawing of a Dreiding model of one enantiomer of a tetrahedral MC–TM complex, reveals stringent restrictions on the MC that may achieve this geometry. With both the 14-P_4 and 14-P_3S ligands, the tetrahedral geometry is possibly only with isomers that we have never observed,[4b] those that have phenyl substituents anti across the benzo fusion. Thus, none of the isomers of 14-P_4 and 14-P_3S we used in this work are capable of giving **15**. Only *c*-PSPS and *t*-PSSP can form the tetrahedral complex **15**.

The electrochemical data obtained in this work are presented in Table IV. This cyclic voltammetric (CV) work was carried out in acetonitrile with a platinum working electrode, a silver/silver nitrate reference electrode, and tetrabutylammonium perchlorate as the supporting electrolyte. Only with the nickel complexes were any reversible peaks observed; [*c*-PSPS·Ni][ClO_4]$_2$ and [*t*-P_3S·Ni(NCMe)][ClO_4]$_2$ gave reversible one-electron reduction waves at −0.89 and −0.94 V, respectively. All other electrochemical processes were either completely irreversible or quasi-reversible. When chloride ion was present in the electrolyte, better reversibility was observed, particularly with those ligands that were capable of giving tetrahedral geometry (*c*-PSPS). At present, it is difficult to rationalize the peak potentials and their reversibilities or lack thereof as a function of the specific ligand. Possibly, the MC exerts counteracting effects on the electron density at the metal center and on the relative stabilities of the oxidized and reduced intermediates formed with the structurally altered MC investigated in this series.

It is of interest to compare our data with those of Warren and Bennett,[21b] who reported for complex **16** an irreversible two-

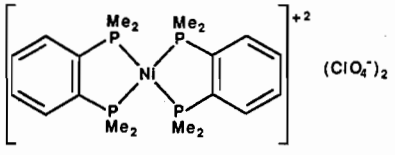

16

electron reduction wave at −1.16 V (vs. Ag/$AgClO_4$). In our hands, **16** also exhibited an irreversible two-electron reduction wave measured by coulometry at −1.20 V (vs. Ag/$AgNO_3$). However, in several cases the MC fosters a completely *reversible* one-electron reduction. It is also interesting to note that only for the *c*-P_4 complex is the second reduction wave quasi-reversible, presumably leading to the Ni(0) species. This is in spite of the fact that the *c*-P_4 ligand is not capable of achieving tetrahedral geometry (vide supra).

The CV work carried out in the presence of chloride ion undoubtedly involved pentacoordinate [MC·NiCl]$^+$ species, as we have discussed above. The reduction waves appeared to be much more reversible, and in addition, the oxidation processes were much better defined as compared to those in the absence of Cl^-. In several cases two oxidation waves are observed, presumably to give Ni(III) and Ni(IV) species.[21b,23]

The CV reductions of the MC–Pd(II) and MC–Pt(II) complexes occur at more anodic potentials than the MC–Ni(II) complexes, as has been observed for other phosphine and arsine complexes of these metal ions.[21b,23] There was essentially no reversibility in the chloride-free CV processes and only some quasi-reversibility with anodic and cathodic processes in the presence of chloride, with no readily apparent trends as a function of MC.

Table IV. Cyclic Voltammetric Peak Potentials (V) of [MC–TM]$(X)_2$

	$E_{p,c}$[a]	$E_{p,a}$[a]	$E_{p,c}/Cl^-$[b]	$E_{p,a}/Cl^-$[b]
[*c*-PPSS·Ni]$(ClO_4)_2$	−1.59	+1.52	−1.53 (q)[c]	−1.44 (q)
	−0.90		−1.24 (r)[c]	−1.17 (r)
			+0.10 (q)	+0.54 (q)
			+1.30 (q)	+1.66 (q)
				+1.35[d]
[*c*-PSPS·Ni]$(ClO_4)_2$	−1.43		−1.42 (q)	−1.38 (q)
	−0.89 (r)	−0.84 (r)	−1.13 (q)	−0.98 (q)
		+1.31	+0.97 (q)	+1.08 (q)
			+1.36 (q)	+1.48 (q)
[*t*-P_3S·Ni]$(ClO_4)_2$	−1.57	−1.42 (q)[d]	−1.55 (q)	−1.45 (q)
	−0.94 (r)	−0.88 (r)	−1.18 (r)	−1.12 (r)
		−0.58[d]		+0.51
		+1.20[d]		+1.09
				+1.57[d]
[*c*-P_3S·Ni]$(ClO_4)_2$	−1.42		−1.43 (q)	−1.36 (q)
	−1.19 (q)	−1.17 (q)	−1.13 (q)[d]	−0.78 (q)
		+1.12		+0.57
		+1.52	+1.18 (q)	+1.22 (q)
				+1.52
[*c*-P_4·Ni]$(ClO_4)_2$	−1.59 (q)	−1.27 (q)	−1.67 (q)	−1.62 (q)
	−1.01		−1.11	+0.87
				+1.87
[*t*-PPSS·Ni]$(ClO_4)_2$	−1.76	+0.97	−1.19 (q)	−1.02 (q)
	−0.97		−0.92	+1.20[d]
				+1.82
[*t*-PSPS·Ni]$(ClO_4)_2$	−1.72	−1.03 (q)	−1.22 (q)	−1.09 (q)
	−1.21 (q)	+1.42 (q)	−0.89 (q)	−0.82 (q)
	+1.21 (q)		+0.97 (q)	+1.04 (q)
[*c*-PPSS·Pd]$(PF_6)_2$	−1.30	−0.35	−1.25 (q)	−0.92 (q)
[*c*-PSPS·Pd]$(ClO_4)_2$	−1.17	+0.54	−1.13	+1.00
		+1.53	+1.02 (q)	+1.25 (q)
	−0.42 (q)[d]	−0.32 (q)[d]		
[*c*-P_3S·Pd]$(PF_6)_2$	−1.46	none	−1.25	none
[*c*-PPSS·Pt]$(ClO_4)_2$	−1.73	none	−1.72	
			+0.16 (q)	+0.62 (q)
			+0.92 (q)	+1.07 (q)
[*c*-PSPS·Pt]$(PF_6)_2$	−1.68	+1.02	−1.63	+0.90
		−1.60 (q)[d]	+0.05	
		−0.14[d]		
		+0.14[d]		
		+1.09[d]		
[*t*-P_3S·Pt]$(BPh_4)_2$	−1.52	+0.54	−1.49 (q)	−1.41 (q)
			−0.49 (q)[d]	−0.38 (q)[d]
			+0.44 (q)	+0.68 (q)
			+0.97 (q)	+1.26 (q)
[*c*-P_3S·Pt]$(PF_6)_2$	−1.86	none	−1.87	−1.11
			−0.07	
[*c*-PSSP·Pt]$(PF_6)_2$	*e*	*e*	−1.40 (q)	−1.10 (q)

[a] $E_{p,c}$ and $E_{p,a}$ are cathodic and anodic peak potentials vs. Ag/0.1 M $AgNO_3$ in CH_3CN. Scan rate = 50 mV/s, unless otherwise noted. [b] $E_{p,c}/Cl^-$ = cathodic peak potentials observed in the presence of excess Cl^-. [c] (q) = quasi-reversible wave, (r) = reversible wave. [d] 1000 mV/s. [e] Not soluble.

Experimental Section

General Information. Proton resonance spectra were obtained on a Varian EM-390, a Varian FT-80, or a Nicolet NT360 spectrometer. Proton-decoupled ^{31}P NMR spectra were determined on a Varian FT-80, Bruker WH90, or Nicolet NT360 spectrometer at 32.2, 36.4, or 144.9 MHz, respectively. Chemical shifts are given in parts per million relative to Me_4Si for ^1H and relative to 85% H_3PO_4 for ^{31}P NMR spectra.

(23) Warren, L. F.; Bennett, M. A. *J. Am. Chem. Soc.* **1974**, *96*, 3340.

Table V. Crystallographic Summary for *c*-PSPS·Ni, *c*-P_3S·Pt, *t*-P_3S·NiCl, and *t*-P_3S·Ni(MeCN)

	c-PSPS·Ni	*c*-P_3S·Pt	*t*-P_3S·NiCl	*t*-P_3S·Ni(MeCN)
		A. Crystal Data (−110 °C)[a]		
a, Å	15.882 (5)	13.359 (4)	12.449 (3)	14.909 (6)
b, Å	16.865 (5)	15.308 (3)	21.574 (4)	23.737 (5)
c, Å	12.713 (1)	20.271 (6)	14.002 (9)	11.238 (2)
α, deg	90	90	90	90
β, deg	97.35 (2)	109.31 (2)	97.82 (4)	100.07 (3)
γ, deg	90	90	90	90
V, Å^3	3377.2 (15)	3912.2 (18)	3725.6 (28)	3915.8 (20)
no. of reflcns for cell data	45	45	45	45
2θ range for cell data, deg	18.4–32.5	18.1–24.0	15.1–22.3	15.6–22.0
d_{calcd}, g cm^{-3} (−110 °C)	1.603	1.830	1.575	1.512
d_{measd}, g cm^{-3} (21 °C)	1.611	1.819	1.567	1.523
chemical formula	$C_{30}H_{30}O_8P_2S_2Cl_2NiCH_3CN$	$C_{36}H_{35}F_{12}P_5SPt$	$C_{36}H_{35}O_4P_3SCl_2NiCH_2Cl_2$	$C_{38}H_{38}O_8NP_3SCl_2Ni$
fw	815.30	1077.67	871.17	820.41
crystal system	monoclinic	monoclinic	monoclinic	monoclinic
space group, *Z*	$P2_1/c$ (No. 14), 4	$P2_1/c$ (No. 14), 4	$P2_1/c$ (No. 14), 4	$P2_1/n$ (No. 14), 4
F(000), e	1680	2112	1816	1840
		B. Data Collection (−110 °C)[b]		
λ(Mo Kα), Å	0.71069	0.71069	0.71069	0.71069
mode	ω scan	ω scan	ω scan	ω scan
scan range		symmetrical over 1.0° about K$\alpha_{1,2}$ max		
background		offset 1.0 and −1.0° in ω from K$\alpha_{1,2}$ max		
scan rate, deg min^{-1}	3.0–6.0	3.0–6.0	3.0–6.0	3.0–6.0
2θ range, deg	4.0–55.0	4.0–55.0	4.0–55.0	4.0–55.0
exposure time, h	101.4	118.4	112.5	117.0
stability: computed, *s*, *t*; cor range (on *I*)	−0.000 027, 0.000 002; 0.98–1.00	−0.000 217, 0.000 001; 1.00–1.01	−0.000 218, 0.000 002; 1.00–1.01	−0.000 074, 0.000 001; 1.00–1.01
no. of total reflcns measd	7776	8975	8557	9013
data crystal vol, mm^3	0.0107	0.0028	0.0055	0.0101
data crystal faces	{11$\bar{1}$}, {001}, 13$\bar{3}$, $\bar{1}$33	{010}, 11$\bar{1}$, $\bar{1}\bar{1}$1, 112, $\bar{1}\bar{1}\bar{2}$, $\bar{2}$11, 2$\bar{1}\bar{1}$	{100}, 01$\bar{1}$, 0$\bar{1}$1, 0$\bar{2}\bar{1}$, 021	{010}, 1$\bar{1}$0, $\bar{1}$10, 011, 0$\bar{1}\bar{1}$
abs coeff, μ(Mo Kα), cm^{-1}	9.99	39.59	10.33	8.57
transmn factor range	0.725–0.948	0.641–0.771	0.834–0.901	0.809–0.912
		C. Structure Refinement[c]		
ignorance factor, *p*	0.02	0.02	0.02	0.02
reflcns used, $F_o \geq n\sigma(F_o)$	6335, 4.0	6954, 4.0	5116, 4.0	6706, 4.0
no. of variables	460	520	483	480
R, R_w	0.041, 0.039	0.052, 0.047	0.063, 0.051	0.043, 0.038
R, R_w for all data	0.058, 0.042	0.072, 0.051	0.120, 0.064	0.067, 0.0463
goodness of fit, *S*	2.05	2.19	1.63	1.70
max shift/esd	0.65	0.17	1.05	0.02
max peak in diff map, e Å^{-3}	0.85	6.6 (near Pt)	1.00	0.80

[a] Unit cell parameters were obtained by least-squares refinement vs. the number of reflections shown, in the 2θ range given. Crystal densities were measured by flotation in an aqueous $ZnCl_2$ solution. [b] Syntex $P2_1$ autodiffractometer with a graphite monochromator and a Syntex LT-1 inert-gas (N_2) low-temperature delivery system. Data reduction was carried out as described in: Riley, P. E.; Davis, R. E. *Acta Crystallogr., Sect B: Struct. Crystallogr. Cryst. Chem.* **1976**, *32*, 381. Crystal and instrument stabilities were monitored by remeasurement of 4 check reflections after every 96 reflections. These data were analyzed as detailed in: Henslee, W. H.; Davis, R. E. *Acta Crystallogr., Sect. B: Struct. Crystallogr. Cryst. Chem.* **1975**, *31*, 1511. [c] Relevant expressions are as follows: function minimized was $\sum w(|F_o| - |F_c|)^2$, where $w = (\sigma|F|)^{-2}$; $R = \sum||F_o| - |F_c||/\sum|F_o|$; $R_w = [\sum w(|F_o| - |F_c|)^2/\sum w|F_o|^2]^{1/2}$; $S = [\sum w(|F_o| - |F_c|)^2/(m - n)]^{1/2}$.

Chemical shifts upfield of the standard are defined as negative. Conductivities were measured on a YSI Model 32 conductance meter using ca. 0.5×10^{-3} M acetonitrile solutions.

The macrocycles used in this work were synthesized as described previously.[4b,g] The ligand 1,2-bis(dimethylphosphino)benzene was prepared as described.[19]

Preparation of MC·NiCl$_2$ Complexes. A typical procedure is given for *c*-PSPS·$NiCl_2$.

(*cis*-6,17-Diphenyl-6,17-diphospha-2,13-dithiatricyclo[16.4.0.0^{7,12}]docosa-7(12),8,10,1(18),19,21-hexaene-κ^2S,κ^2P)nickel Dichloride.[24] A solution of *c*-PSPS (60 mg, 0.117 mmol) in CH_2Cl_2 (2 mL) was added to a stirred solution of $NiCl_2·6H_2O$ (28 mg, 0.117 mmol) in EtOH (0.5 mL) at room temperature to give a brown solution. To this was added ether (2 mL), and the resulting solution was allowed to stand for 24 h at −20 °C and then filtered to give *c*-PSPS·$NiCl_2$ as a yellow solid (55 mg, 73%). The physical properties for this and related complexes are given in Table I.

Preparation of [MC·Ni](ClO$_4$)$_2$ Complexes. A typical procedure is given for [*c*-PSPS·Ni]$(ClO_4)_2$.

(*cis*-6,17-Diphenyl-6,17-diphospha-2,13-dithiatricyclo[16.4.0.0^{7,12}]docosa-7(12),8,10,1(18),19,21-hexaene-κ^2S,κ^2P)nickel Diperchlorate.[24] A solution of *c*-PSPS (78.3 mg, 0.152 mmol) in THF (1 mL) was added to a stirred solution of $Ni(ClO_4)_2·6H_2O$ (58.5 mg, 0.156 mmol) in EtOH (0.5 mL) at room temperature. The resulting mixture was stirred for 0.5 h and then filtered to give a yellow powder (98 mg), which was recrystallized from acetonitrile to give the title complex as analytically pure yellow-orange crystals (90 mg, 76%) from which a single crystal suitable for X-ray analysis was chosen. The physical properties for this and related complexes are given in Table I.

Preparation of [MC·NiCl](ClO$_4$) Complexes. A typical procedure is given for [*t*-P_3S·NiCl](ClO_4).

(*cis*,*trans*-6,13,17-Triphenyl-6,13,17-triphospha-2-thiatricyclo[16.4.0.0^{7,12}]docosa-7(12),8,10,1(18),19,21-hexaene-$\kappa S,\kappa^3P$)nickel Chloride Perchlorate. A solution of $NiCl_2·6H_2O$ (30.2 mg, 0.127 mmol) and $Ni(ClO_4)_2·6H_2O$ (46.2 mg, 0.123 mmol) in 95% ethanol (3 mL) was added to *t*-P_3S (145.5 mg, 0.246 mmol) in CH_2Cl_2 (3 mL). The solution was concentrated, and the residue was redissolved in ethanol/dichloromethane (2 mL, 1:1, v/v). This solution was cooled to −20 °C for 24 h to give the title complex as analytically pure, intensely dark green crystals (99 mg, 46%), from which a crystal suitable for X-ray analysis was chosen. The physical properties of this and related complexes are given in Table I.

Preparation of [MC·Pt^{II}] or [MC·Pd^{II}](X)$_2$ Complexes. A typical procedure is given for [*c*-PSSP·Pt^{II}]$(ClO_4)_2$.

(*cis*-13,17-Diphenyl-13,17-diphospha-2,6-dithiatricyclo[16.4.0.0^{7,12}]-docosa-7(12),8,10,1(18),19,21-hexaene-κ^2S-κ^2P)platinum Diperchlorate. A solution of (1,5-cyclooctadiene)platinum(II) dichloride (73.6 mg, 0.197 mmol) in CH_2Cl_2 (5 mL) was added to a stirred solution of *c*-PSSP (98.4

(24) For a description of the "κ" nomenclature, see: Sloan, T. E.; Busch, D. H. *Inorg. Chem.* **1978**, *17*, 2043.

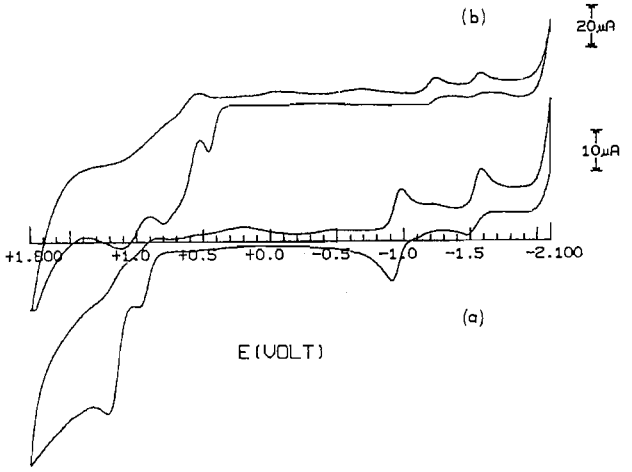

Figure 3. Cyclic voltammograms of $[t\text{-}P_3S\cdot Ni](ClO_4)_2$ in 0.1 M TBAP/CH_3CN (platinum-disk working electrode; $Ag/AgNO_3$ reference electrode; scan rate 100 mV/s): (a) prior to addition of excess chloride ion (as TEAC); (b) after addition of excess chloride ion. The oxidative wave at +0.6 V in (b) is due to oxidation of chloride ion.

mg, 0.191 mmol) in CH_2Cl_2 (2 mL). The murky solution was treated with 95% ethanol (2 mL) to give a clear solution, to which was added silver perchlorate (81.9 mg, 0.395 mmol) in 95% ethanol. The resulting mixture was stirred for 2 h, filtered, and concentrated. The residue was recrystallized from acetonitrile to give the title complex as colorless crystals (40 mg, 23%). The physical properties of this and related platinum and palladium complexes are given in Table I.

Stability of $[t\text{-PSSP}\cdot Ni](ClO_4)_2$ in Acetonitrile. A solution of the title complex (4.64 mg, 6.00×10^{-3} mmol) in acetonitrile (3.00 mL) was allowed to stand at room temperature for 14 h, at which point only 25% of the original complex was present as determined by UV spectroscopy (λ_{max} 550 and 416 nm were monitored). A ^{31}P NMR spectrum of the concentrated sample revealed the presence of the uncomplexed macrocycle.

Stability of $[MC\cdot Ni](ClO_4)_2$ Complexes in Pyridine. Two typical runs are described.

$[c\text{-PSSP}\cdot Ni](ClO_4)_2$ in Pyridine. The title complex (7.0 mg, 9.0×10^{-3} mmol) was dissolved in pyridine (0.70 mL), and a ^{31}P NMR spectrum was taken 1.0 h following dissolution, at which time the peak height ratio of the complexed (+41.8 ppm) and uncomplexed (−25.3 ppm) ligands was 82:18. In 6 h, the corresponding ratio was 63:37; after 18 h, it was 58:42 and did not change further as a function of time.

$[c\text{-PSPS}\cdot Ni](ClO_4)_2$ in Pyridine. The title complex (6.7 mg, 8.7 mmol) was dissolved in pyridine (0.7 mL). A ^{31}P NMR spectrum of the somewhat murky solution showed an absorption only for the free ligand (−22.9 ppm).

Other stabilities were determined similarly, and the results are summarized in Scheme I.

Stability of $[c\text{-}P_3S\cdot Ni](ClO_4)_2$ toward 1,2-Bis(dimethylphosphino)benzene. The title complex (6.8 mg, 8.0×10^{-3} mmol) was dissolved in acetonitrile (0.7 mL), then 1,2-bis(dimethylphosphino)benzene (15 mg, 76×10^{-3} mmol) was added, and the solution was allowed to stand in an NMR tube for 2 h. At this time the ^{31}P NMR spectrum featured absorptions due to $\{[1,2\text{-}(Me_2P)_2C_6H_4]Ni\}(ClO_4)_2$ (39.8 ppm), 1,2-$(Me_2P)_2C_6H_4$ (−55.9 ppm), and $c\text{-}P_3S$ (−25.0 (d, J = 5 Hz), −25.6 (s), −26.1 (d, J = 5 Hz) ppm) but no absorptions due to the original complex (see Table I).

A similar experiment was carried out for $[c\text{-}P_4\cdot Ni](ClO_4)_2$ in which the rate of equilibration was much slower than that for the $c\text{-}P_3S$ complex. About 1 week was required to establish an equilibrium. The equilibrium constant was about 10^{-1}.

Electrochemistry. Electrochemically pure acetonitrile was prepared according to the method of O'Donnell, Ayres, and Mann.[25] Acetonitrile was distilled rapidly from a mixture of anhydrous sodium carbonate and potassium permanganate (10 g of Na_2CO_3 and 15 g of $KMnO_4$ added to 800 mL of CH_3CN). The distillate was acidified with concentrated H_2SO_4, decanted from the resultant white precipitate, and then distilled at 5–10 mL/h through a column packed with glass helices. A 5% forecut was discarded. This resulted in CH_3CN, which was electrochemically pure over a minimum solvent window of +1.6 to −2.3 V vs. Ag/0.1 M $AgNO_3$ in acetonitrile. Alternatively, Fisher HPLC grade acetonitrile, which displayed essentially the same solvent window, was used as received. Anhydrous tetra-*n*-butylammonium perchlorate (TBAP) was recrystallized twice from hexane/ethyl acetate and dried for 24 h under vacuum. Tetraethylammonium chloride (TEAC) was recrystallized twice from methanol and dried for 24 h under vacuum. Ferrocene was purified by sublimation prior to use.

Cyclic voltammetry was performed by using a Bioanalytical Systems BAS-100 electrochemical analyzer and a Houston Instruments Hiplot DMP-40 digital plotter. The cell used was a one-compartment microcell, approximate volume 0.5 mL, with a platinum-disk working electrode and a platinum-wire auxiliary electrode sealed into the side and bottom of the cell, respectively. The microcell was equipped with a silver wire/0.1 M silver nitrate in acetonitrile reference electrode and connected to the microcell through a salt bridge. TBAP (0.1 M in CH_3CN) was used as the supporting electrolyte. Approximately 0.1 mL of a solution of 0.1 M TEAC in CH_3CN was added to the electrolyte solution as a source of chloride ion when desired. All solutions were deaerated with dry argon for at least 15 min prior to obtaining the voltammograms. Positive feedback for IR compensation to minimize the effect of solution resistance was utilized in all experiments. The cyclic voltammetric scan rate was either 50 or 100 mV/s unless otherwise noted.

All potentials reported herein are referenced to a $Ag/AgNO_3$ reference electrode. The ferrocene/ferrocenium couple displays a one-electron

(25) O'Donnell, J. F.; Ayres, J. T.; Mann, C. K. *Anal. Chem.* **1965**, *37*, 1161.

Table VI. Fractional Coordinates and Isotropic or Equivalent Isotropic[a] Thermal Parameters (Å^2) for Non-Hydrogen Atoms of $[c\text{-PSPS}\cdot Ni][ClO_4]_2\cdot CH_3CN$

atom	x	y	z	U
Ni	0.75176 (2)	0.96194 (2)	0.76871 (3)	0.01789 (10)
P1	0.88189 (4)	1.00475 (4)	0.76930 (5)	0.0178 (2)
P2	0.62243 (4)	0.91891 (4)	0.76935 (6)	0.0213 (2)
S1	0.70766 (4)	1.07973 (4)	0.79880 (5)	0.0205 (2)
S2	0.79371 (4)	0.84650 (4)	0.72016 (5)	0.0220 (2)
C1	0.9189 (2)	1.0685 (2)	0.8814 (2)	0.0234 (9)
C2	0.8615 (2)	1.1405 (2)	0.8893 (2)	0.0246 (9)
C3	0.7728 (2)	1.1220 (2)	0.9149 (2)	0.0245 (9)
C4	0.6167 (2)	0.8276 (2)	0.8441 (2)	0.0284 (9)
C5	0.6636 (2)	0.7602 (2)	0.7956 (3)	0.0329 (10)
C6	0.7596 (2)	0.7686 (2)	0.8064 (2)	0.0285 (9)
C7	0.9064 (2)	0.8451 (2)	0.7608 (2)	0.0226 (8)
C8	0.9477 (2)	0.9175 (2)	0.7820 (2)	0.0218 (8)
C9	1.0350 (2)	0.9182 (2)	0.8138 (2)	0.0275 (9)
C10	1.0795 (2)	0.8475 (2)	0.8248 (2)	0.0324 (10)
C11	1.0378 (2)	0.7765 (2)	0.8033 (3)	0.0350 (11)
C12	0.9513 (2)	0.7748 (2)	0.7694 (3)	0.0313 (10)
C13	0.6060 (2)	1.0687 (2)	0.8436 (2)	0.0252 (9)
C14	0.5650 (2)	0.9966 (2)	0.8289 (2)	0.0237 (9)
C15	0.4820 (2)	0.9890 (2)	0.8534 (2)	0.0322 (10)
C16	0.4427 (2)	1.0536 (2)	0.8916 (3)	0.0387 (12)
C17	0.4841 (2)	1.1252 (2)	0.9058 (3)	0.0374 (12)
C18	0.5663 (2)	1.1344 (2)	0.8819 (3)	0.0323 (11)
C19	0.90211 (8)	1.05779 (7)	0.65108 (10)	0.0206 (8)
C20	0.98461 (8)	1.06608 (7)	0.62592 (10)	0.0322 (10)
C21	0.99941 (8)	1.10943 (7)	0.53665 (10)	0.0387 (12)
C22	0.93170 (8)	1.14449 (7)	0.47253 (10)	0.0356 (11)
C23	0.84920 (8)	1.13620 (7)	0.49769 (10)	0.0348 (11)
C24	0.83440 (8)	1.09284 (7)	0.58697 (10)	0.0279 (9)
C25	0.56577 (9)	0.90028 (8)	0.63958 (10)	0.0236 (9)
C26	0.60115 (9)	0.92633 (8)	0.55076 (10)	0.0301 (10)
C27	0.55717 (9)	0.91568 (8)	0.44955 (10)	0.0373 (11)
C28	0.47781 (9)	0.87897 (8)	0.43714 (10)	0.0404 (12)
C29	0.44243 (9)	0.85291 (8)	0.52595 (10)	0.0399 (11)
C30	0.48641 (9)	0.86357 (8)	0.62717 (10)	0.0337 (10)
Cl1	0.68203 (4)	1.29641 (4)	0.67843 (6)	0.0271 (2)
Cl2	0.81517 (5)	0.88482 (5)	1.06708 (6)	0.0371 (3)
O5	0.7532 (2)	0.8283 (2)	1.0795 (2)	0.0752 (12)
O6	0.8547 (2)	0.9105 (2)	1.1666 (2)	0.0765 (13)
O7	0.7776 (3)	0.9420 (2)	1.0009 (4)	0.162 (3)
O8	0.8784 (2)	0.8535 (4)	1.0149 (4)	0.176 (3)
O1	0.72357 (15)	1.24392 (14)	0.6129 (2)	0.0440 (9)
O2	0.6925 (2)	1.37643 (14)	0.6450 (2)	0.0459 (9)
O3	0.7169 (2)	1.2879 (2)	0.7866 (2)	0.0613 (11)
O4	0.59342 (15)	1.2789 (2)	0.6668 (2)	0.0571 (10)
N1	0.7903 (2)	0.6007 (2)	0.9538 (3)	0.0645 (14)
CS1	0.7700 (2)	0.5531 (2)	0.8935 (3)	0.0438 (13)
CS2	0.7423 (3)	0.4916 (3)	0.8161 (3)	0.059 (2)

[a] For anisotropic atoms, the U value is U_{eq} calculated as $U_{eq} = {}^1/_3\sum_i\sum_j U_{ij}a_i^*a_j^*A_{ij}$, where A_{ij} is the dot product of the ith and jth direct-space unit cell vectors.

Table VII. Fractional Coordinates and Equivalent Isotropic[a] Thermal Parameters (Å^2) for Non-Hydrogen Atoms of $[c\text{-}P_3S\cdot Pt][PF_6]_2$

atom	x	y	z	U
Pt	0.26104 (2)	0.06506 (2)	0.262602 (15)	0.01831 (9)
S	0.3045 (2)	0.20985 (12)	0.25264 (9)	0.0230 (6)
P1	0.2710 (2)	0.03163 (13)	0.15490 (10)	0.0207 (7)
P2	0.2772 (2)	0.09360 (13)	0.37621 (10)	0.0216 (7)
P3	0.2355 (2)	−0.07859 (12)	0.27579 (11)	0.0227 (7)
C1	0.3965 (6)	0.0713 (5)	0.1486 (4)	0.026 (3)
C2	0.4096 (7)	0.1716 (5)	0.1585 (4)	0.026 (3)
C3	0.4269 (6)	0.2050 (5)	0.2312 (4)	0.025 (3)
C4	0.3621 (6)	0.0154 (5)	0.4355 (4)	0.026 (3)
C5	0.3230 (7)	−0.0790 (5)	0.4236 (4)	0.028 (3)
C6	0.3282 (7)	−0.1207 (5)	0.3554 (4)	0.027 (3)
C7	0.2612 (6)	−0.1350 (5)	0.2049 (4)	0.021 (3)
C8	0.2741 (6)	−0.0865 (5)	0.1494 (4)	0.021 (3)
C9	0.2931 (7)	−0.1280 (6)	0.0935 (4)	0.029 (3)
C10	0.2987 (8)	−0.2193 (6)	0.0936 (5)	0.037 (4)
C11	0.2876 (8)	−0.2660 (6)	0.1486 (5)	0.037 (4)
C12	0.2673 (7)	−0.2268 (5)	0.2030 (4)	0.031 (3)
C13	0.3508 (6)	0.2488 (5)	0.3398 (4)	0.025 (3)
C14	0.3432 (6)	0.1975 (5)	0.3953 (4)	0.024 (3)
C15	0.3823 (7)	0.2312 (6)	0.4631 (4)	0.033 (3)
C16	0.4299 (7)	0.3135 (6)	0.4760 (4)	0.036 (3)
C17	0.4348 (8)	0.3635 (6)	0.4199 (5)	0.035 (4)
C18	0.3950 (7)	0.3326 (5)	0.3525 (4)	0.031 (3)
C19	0.1681 (4)	0.0749 (4)	0.0797 (2)	0.023 (3)
C20	0.0697 (4)	0.0943 (4)	0.0860 (2)	0.033 (3)
C21	−0.0111 (4)	0.1287 (4)	0.0292 (2)	0.040 (3)
C22	0.0066 (4)	0.1437 (4)	−0.0339 (2)	0.042 (4)
C23	0.1051 (4)	0.1242 (4)	−0.0402 (2)	0.049 (4)
C24	0.1858 (4)	0.0898 (4)	0.0166 (2)	0.040 (3)
C25	0.1568 (4)	0.1029 (4)	0.3967 (2)	0.025 (3)
C26	0.1562 (4)	0.0933 (4)	0.4650 (2)	0.043 (4)
C27	0.0610 (4)	0.0998 (4)	0.4790 (2)	0.051 (4)
C28	−0.0335 (4)	0.1160 (4)	0.4247 (2)	0.065 (5)
C29	−0.0328 (4)	0.1257 (4)	0.3564 (2)	0.111 (8)
C30	0.0624 (4)	0.1191 (4)	0.3424 (2)	0.079 (6)
C31	0.1051 (4)	−0.1072 (4)	0.2764 (3)	0.028 (3)
C32	0.0902 (4)	−0.1701 (4)	0.3220 (3)	0.055 (5)
C33	−0.0106 (4)	−0.1837 (4)	0.3267 (3)	0.064 (5)
C34	−0.0964 (4)	−0.1343 (4)	0.2856 (3)	0.060 (5)
C35	−0.0815 (4)	−0.0714 (4)	0.2400 (3)	0.117 (8)
C36	0.0192 (4)	−0.0578 (4)	0.2353 (3)	0.080 (6)
P4	0.3863 (2)	0.47203 (14)	0.15811 (11)	0.0262 (7)
F1	0.4124 (4)	0.4130 (3)	0.1006 (2)	0.039 (2)
F2	0.4833 (4)	0.4263 (3)	0.2172 (2)	0.048 (2)
F3	0.3639 (5)	0.5314 (4)	0.2157 (3)	0.051 (2)
F4	0.2923 (5)	0.5168 (4)	0.0983 (3)	0.054 (2)
F5	0.4672 (5)	0.5434 (3)	0.1488 (3)	0.053 (2)
F6	0.3095 (5)	0.3993 (4)	0.1679 (4)	0.067 (3)
P5	0.2800 (2)	−0.3975 (2)	0.38630 (11)	0.0316 (8)
F7	0.3023 (5)	−0.4760 (4)	0.3432 (3)	0.057 (2)
F8	0.3625 (4)	−0.4345 (4)	0.4567 (3)	0.053 (2)
F9	0.1884 (5)	−0.4494 (4)	0.4015 (3)	0.069 (3)
F10	0.1966 (5)	−0.3594 (4)	0.3167 (3)	0.061 (3)
F11	0.3697 (5)	−0.3412 (4)	0.3715 (3)	0.071 (3)
F12	0.2575 (5)	−0.3169 (4)	0.4297 (3)	0.063 (3)

[a] For anisotropic atoms, the U value is U_{eq} calculated as $U_{eq} = {}^1/_3\sum_i\sum_j U_{ij}a_i^*a_j^*A_{ij}$, where A_{ij} is the dot product of the ith and jth direct-space unit cell vectors.

reversible wave centered at +0.045 V vs. this electrode compared with +0.307 V[26] vs. an aqueous saturated calomel electrode.

Typical cyclic voltammograms are shown in Figure 3 for the complex $[t\text{-}P_3S\cdot Ni](ClO_4)_2$ in the absence and presence of chloride ion. The wave at +0.6 V in Figure 3b is due to oxidation of excess chloride ion. Constant-potential coulometry of $[t\text{-}P_3S\cdot Ni](ClO_4)_2$ indicated that the first reduction wave was a one-electron process, presumably to give the corresponding Ni(I) species. Determination of the n values of the other reductive and oxidative waves proved difficult, however. Chronocoulometric experiments, as well as an inability to pass more than a small fraction of the expected amount of charge during coulometric experiments, indicated that for many of these processes passivation of the electrode surface occurred, thereby preventing further electron transfer.

Controlled-potential coulometry experiments were conducted by using an Electrosynthesis Company (ESC) Model 420X power supply, an ESC Model 415 potentiostatic controller, and an ESC Model 640 digital coulometer. Current–time curves were recorded on a Houston Instruments Model 2000 X-Y-T recorder. The coulometry cell used was a two-compartment cell equipped with reticulated-vitreous-carbon (RVC) (The Electrosynthesis Co., porosity = 80 pores/in.) working and auxiliary electrodes and an $Ag/AgNO_3$ reference electrode. The auxiliary electrode was isolated from the working-electrode compartment by a Corning fine glass frit. Cyclic voltammograms obtained by using a glassy-carbon working electrode were used to determine the proper electrolysis potentials with the graphite-felt or RVC electrodes. In all cases, electrolysis potentials were chosen corresponding to the diffusion-limited portions of the cyclic voltammetric waves. TBAP (0.2 M in CH_3CN) was used as the supporting electrolyte, and all solutions were deaerated with dry argon prior to electrolysis. Supporting electrolyte solutions were preelectrolyzed to remove electroactive impurities. The end point of the coulometric experiments was taken to be the point at which the current decay reached background levels.

Table VIII. Fractional Coordinates and Equivalent Isotropic[a] Thermal Parameters (Å^2) for Non-Hydrogen Atoms of $[t\text{-}P_3S\cdot NiCl][ClO_4]\cdot CH_2Cl_2$

atom	x	y	z	U
Ni	0.13268 (6)	0.08660 (3)	0.23227 (5)	0.0184 (2)
P1	0.30845 (11)	0.08448 (6)	0.26101 (10)	0.0204 (4)
P2	0.02749 (11)	0.17051 (6)	0.21842 (10)	0.0198 (4)
P3	0.14238 (11)	0.08270 (6)	0.38583 (9)	0.0185 (4)
Cl1	−0.01448 (11)	0.01690 (6)	0.22152 (10)	0.0283 (4)
S	0.12180 (12)	0.08254 (7)	0.07438 (10)	0.0267 (5)
C1	0.3757 (5)	0.1275 (3)	0.1738 (4)	0.029 (2)
C2	0.3386 (5)	0.1119 (3)	0.0673 (4)	0.033 (2)
C3	0.2225 (5)	0.1333 (3)	0.0314 (4)	0.035 (2)
C4	−0.0740 (4)	0.1740 (3)	0.3004 (4)	0.025 (2)
C5	−0.0199 (4)	0.1733 (2)	0.4065 (4)	0.024 (2)
C6	0.0262 (4)	0.1095 (2)	0.4397 (4)	0.021 (2)
C7	0.2579 (4)	0.1306 (2)	0.4304 (4)	0.020 (2)
C8	0.3412 (4)	0.1284 (2)	0.3725 (4)	0.020 (2)
C9	0.4365 (5)	0.1614 (3)	0.3984 (4)	0.027 (2)
C10	0.4459 (5)	0.1985 (3)	0.4794 (5)	0.031 (2)
C11	0.3639 (5)	0.2024 (3)	0.5352 (4)	0.028 (2)
C12	0.2690 (5)	0.1681 (3)	0.5116 (4)	0.024 (2)
C13	0.0022 (5)	0.1265 (3)	0.0331 (4)	0.027 (2)
C14	−0.0446 (5)	0.1643 (2)	0.0966 (4)	0.023 (2)
C15	−0.1396 (5)	0.1960 (3)	0.0624 (4)	0.029 (2)
C16	−0.1847 (5)	0.1899 (3)	−0.0336 (5)	0.037 (2)
C17	−0.1377 (6)	0.1521 (3)	−0.0955 (5)	0.039 (2)
C18	−0.0441 (5)	0.1192 (3)	−0.0624 (4)	0.035 (2)
C19	0.3816 (3)	0.01227 (14)	0.2780 (2)	0.025 (2)
C20	0.3535 (3)	−0.03501 (14)	0.2113 (2)	0.036 (2)
C21	0.4070 (3)	−0.09192 (14)	0.2219 (2)	0.043 (2)
C22	0.4885 (3)	−0.10155 (14)	0.2991 (2)	0.041 (2)
C23	0.5166 (3)	−0.05427 (14)	0.3658 (2)	0.041 (2)
C24	0.4631 (3)	0.00264 (14)	0.3552 (2)	0.034 (2)
C25	0.0859 (2)	0.2489 (2)	0.2254 (2)	0.021 (2)
C26	0.1953 (2)	0.2564 (2)	0.2610 (2)	0.027 (2)
C27	0.2398 (2)	0.3157 (2)	0.2720 (2)	0.032 (2)
C28	0.1749 (2)	0.3675 (2)	0.2474 (2)	0.035 (2)
C29	0.0655 (2)	0.3600 (2)	0.2118 (2)	0.033 (2)
C30	0.0210 (2)	0.3007 (2)	0.2008 (2)	0.031 (2)
C31	0.1785 (3)	0.00766 (14)	0.4400 (2)	0.022 (2)
C32	0.1875 (3)	−0.04411 (14)	0.3819 (2)	0.027 (2)
C33	0.2277 (3)	−0.09973 (14)	0.4232 (2)	0.033 (2)
C34	0.2591 (3)	−0.10357 (14)	0.5225 (2)	0.038 (2)
C35	0.2501 (3)	−0.05180 (14)	0.5806 (2)	0.035 (2)
C36	0.2098 (3)	0.00382 (14)	0.5393 (2)	0.029 (2)
Cl2	0.62509 (12)	0.27159 (6)	0.72055 (11)	0.0300 (4)
O1	0.6573 (3)	0.3260 (2)	0.7745 (3)	0.047 (2)
O2	0.7128 (3)	0.2286 (2)	0.7247 (3)	0.042 (2)
O3	0.5318 (4)	0.2447 (2)	0.7509 (4)	0.061 (2)
O4	0.5957 (4)	0.2907 (2)	0.6212 (3)	0.070 (2)
Cl3	0.3612 (3)	0.0014 (2)	−0.1708 (3)	0.080 (2)
Cl4	0.3766 (3)	−0.0724 (2)	−0.0084 (3)	0.083 (2)
CS	0.2983 (7)	−0.0555 (4)	−0.1130 (6)	0.071 (3)
CS1	0.2338 (8)	−0.0121 (7)	−0.0695 (12)	0.219 (9)

[a] For anisotropic atoms, the U value is U_{eq} calculated as $U_{eq} = {}^1/_3\sum_i\sum_j U_{ij}a_i^*a_j^*A_{ij}$, where A_{ij} is the dot product of the ith and jth direct-space unit cell vectors.

(26) Bard, A. J.; Faulkner, L. R. *Electrochemical Methods*; Wiley: New York, 1980; p 701.

Table IX. Fractional Coordinates and Equivalent Isotropic[a] Thermal Parameters (Å^2) for Non-Hydrogen Atoms of $[t\text{-}P_3S\text{-}Ni(NCCH_3)][ClO_4]_2$

atom	x	y	z	U
Ni	0.84230 (2)	0.135870 (15)	0.12997 (3)	0.02210 (11)
S	0.98931 (5)	0.12233 (3)	0.19579 (6)	0.0260 (2)
P1	0.80731 (5)	0.07317 (3)	0.25658 (6)	0.0226 (2)
P2	0.87141 (5)	0.22315 (3)	0.08944 (7)	0.0253 (2)
P3	0.69811 (5)	0.15122 (3)	0.07847 (6)	0.0233 (2)
C1	0.8711 (2)	0.08395 (13)	0.4086 (2)	0.0277 (9)
C2	0.9747 (2)	0.08213 (13)	0.4205 (3)	0.0316 (10)
C3	1.0167 (2)	0.13016 (13)	0.3597 (3)	0.0313 (10)
C4	0.8029 (2)	0.24788 (13)	−0.0501 (3)	0.0316 (10)
C5	0.7040 (2)	0.25949 (13)	−0.0374 (3)	0.0344 (11)
C6	0.6629 (2)	0.22412 (12)	0.0547 (3)	0.0299 (10)
C7	0.6418 (2)	0.12498 (12)	0.1971 (2)	0.0243 (9)
C8	0.6905 (2)	0.08553 (12)	0.2751 (2)	0.0246 (9)
C9	0.6497 (2)	0.05990 (13)	0.3641 (3)	0.0300 (10)
C10	0.5617 (2)	0.07436 (14)	0.3744 (3)	0.0343 (11)
C11	0.5136 (2)	0.11364 (14)	0.2968 (3)	0.0350 (11)
C12	0.5532 (2)	0.13883 (14)	0.2085 (3)	0.0321 (10)
C13	1.0440 (2)	0.18114 (12)	0.1389 (3)	0.0271 (9)
C14	0.9912 (2)	0.22363 (12)	0.0785 (3)	0.0284 (10)
C15	1.0337 (2)	0.26646 (15)	0.0247 (3)	0.0389 (12)
C16	1.1271 (3)	0.2668 (2)	0.0351 (4)	0.0449 (13)
C17	1.1790 (2)	0.2251 (2)	0.0995 (3)	0.0423 (13)
C18	1.1379 (2)	0.18154 (15)	0.1503 (3)	0.0339 (11)
C19	0.81902 (14)	−0.00094 (8)	0.22036 (13)	0.0248 (9)
C20	0.84322 (14)	−0.04197 (8)	0.30904 (13)	0.0318 (10)
C21	0.85578 (14)	−0.09765 (8)	0.27576 (13)	0.0394 (11)
C22	0.84414 (14)	−0.11230 (8)	0.15381 (13	0.0416 (12)
C23	0.81994 (14)	−0.07127 (8)	0.06514 (13)	0.0440 (12)
C24	0.80738 (14)	−0.01559 (8)	0.09841 (13)	0.0335 (10)
C25	0.86559 (15)	0.27834 (7)	0.2002 (2)	0.0290 (10)
C26	0.86673 (15)	0.26469 (7)	0.3212 (2)	0.0371 (11)
C27	0.87402 (15)	0.30721 (7)	0.4080 (2)	0.0471 (13)
C28	0.88017 (15)	0.36339 (7)	0.3738 (2)	0.0484 (13)
C29	0.87902 (15)	0.37704 (7)	0.2528 (2)	0.0438 (13)
C30	0.87174 (15)	0.33451 (7)	0.1660 (2)	0.0353 (11)
C31	0.6482 (2)	0.11161 (8)	−0.05516 (15)	0.0279 (9)
C32	0.6065 (2)	0.05992 (8)	−0.04189 (15)	0.0391 (11)
C33	0.5729 (2)	0.02754 (8)	−0.14352 (15)	0.0489 (14)
C34	0.5810 (2)	0.04685 (8)	−0.25841 (15)	0.0482 (13)
C35	0.6227 (2)	0.09854 (8)	−0.27168 (15)	0.0537 (15)
C36	0.6563 (2)	0.13092 (8)	−0.17005 (15)	0.0466 (13)
Cl1	0.77367 (5)	0.43841 (3)	−0.11854 (7)	0.0338 (2)
Cl2	0.92501 (5)	0.20531 (3)	0.68124 (7)	0.0351 (3)
O1	0.3612 (2)	0.04971 (11)	0.4506 (2)	0.055229 (3)
O2	0.2716 (2)	0.05649 (14)	0.2555 (2)	0.0775445 (13)
O3	0.2103 (2)	0.0235 (2)	0.4151 (2)	0.092670 (7)
O4	0.2482 (2)	0.11606 (13)	0.4083 (4)	0.11842 (4)
O5	0.9055 (2)	0.26319 (9)	−0.2971 (2)	0.044428 (2)
O6	0.9834 (2)	0.20082 (13)	−0.4054 (3)	0.078546 (12)
O7	0.8425 (2)	0.17683 (12)	−0.3633 (3)	0.09130 (2)
O8	0.9666 (2)	0.17968 (12)	−0.2091 (2)	0.071176 (6)
N	0.8662 (2)	0.09933 (11)	−0.0328 (2)	0.0314 (9)
CS1	0.8886 (2)	0.07795 (14)	−0.1118 (3)	0.0354 (11)
CS2	0.9166 (3)	0.0480 (2)	−0.2128 (4)	0.064 (2)

[a] For anisotropic atoms, the U value is U_{eq} calculated as $U_{eq} = {}^1/_3\sum_i\sum_j U_{ij}a_i^*a_j^*A_{ij}$, where A_{ij} is the dot product of the ith and jth direct-space unit cell vectors.

Table X. Revised Fractional Coordinates and Isotropic or Equivalent Isotropic[a] Thermal Parameters (Å^2) of the Non-Hydrogen Atoms for $[c\text{-}PSPS\text{-}Pt][PF_6]_2\cdot C_6H_6$

atom	x	y	z	U
Pt	0.25619 (2)	0.55267 (2)	0.230303 (15)	0.02017 (8)
P1	0.2342 (2)	0.53537 (12)	0.33639 (9)	0.0232 (7)
P2	0.2479 (2)	0.56630 (13)	0.11890 (9)	0.0254 (7)
S1	0.21179 (15)	0.69808 (12)	0.22923 (9)	0.0243 (6)
S2	0.3012 (2)	0.40789 (12)	0.23276 (10)	0.0271 (6)
C1	0.1024 (6)	0.5802 (5)	0.3402 (4)	0.030 (3)
C2	0.0911 (7)	0.6770 (5)	0.3243 (4)	0.031 (3)
C3	0.0803 (6)	0.7004 (6)	0.2523 (4)	0.032 (3)
C4	0.1781 (7)	0.4754 (5)	0.0693 (4)	0.031 (3)
C5	0.2322 (8)	0.3874 (5)	0.0939 (4)	0.036 (3)
C6	0.2144 (7)	0.3542 (5)	0.1594 (4)	0.034 (3)
C7	0.2490 (6)	0.3628 (5)	0.2997 (4)	0.029 (3)
C8	0.2275 (6)	0.4188 (4)	0.3481 (4)	0.026 (3)
C9	0.1980 (7)	0.3822 (6)	0.4024 (4)	0.033 (3)
C10	0.1859 (6)	0.2931 (5)	0.4076 (4)	0.036 (3)
C11	0.2050 (7)	0.2386 (5)	0.3569 (4)	0.039 (3)
C12	0.2381 (6)	0.2728 (5)	0.3035 (4)	0.030 (3)
C13	0.1638 (6)	0.7251 (5)	0.1421 (4)	0.027 (3)
C14	0.1704 (6)	0.6652 (5)	0.0931 (3)	0.025 (3)
C15	0.1255 (7)	0.6871 (6)	0.0267 (4)	0.033 (3)
C16	0.0748 (7)	0.7674 (6)	0.0103 (4)	0.035 (3)
C17	0.0732 (7)	0.8289 (6)	0.0599 (4)	0.036 (3)
C18	0.1178 (6)	0.8078 (5)	0.1254 (4)	0.034 (3)
CA2	0.3076 (3)	0.6206 (3)	0.4591 (2)	0.039 (3)
CA3	0.3881 (3)	0.6535 (3)	0.5127 (2)	0.045 (3)
CA4	0.4985 (3)	0.6448 (3)	0.5137 (2)	0.042 (3)
CA5	0.5283 (3)	0.6032 (3)	0.4610 (2)	0.041 (3)
CA6	0.4478 (3)	0.5704 (3)	0.4074 (2)	0.033 (3)
CA1	0.3374 (3)	0.5791 (3)	0.4064 (2)	0.025 (2)
CB2	0.4750 (4)	0.5604 (3)	0.1451 (2)	0.037 (3)
CB3	0.5753 (4)	0.5692 (3)	0.1291 (2)	0.039 (3)
CB4	0.5785 (4)	0.5954 (3	0.0651 (2)	0.043 (3)
CB5	0.4812 (4)	0.6127 (3)	0.0171 (2)	0.045 (4)
CB6	0.3809 (4)	0.6039 (3)	0.0330 (2)	0.037 (3)
CB1	0.3778 (4)	0.5778 (3)	0.0970 (2)	0.026 (3)
P3	−0.1981 (2)	0.58207 (13)	0.38664 (11)	0.0326 (7)
F1	−0.1668 (5)	0.5036 (3)	0.3456 (3)	0.062 (2)
F2	−0.0780 (5)	0.5781 (5)	0.4320 (3	0.106 (3)
F3	−0.2284 (5)	0.6618 (3)	0.4278 (3)	0.083 (3)
F4	−0.1590 (7)	0.6476 (4)	0.3398 (4)	0.128 (5)
F5	−0.3158 (5)	0.5841 (5)	0.3428 (4)	0.129 (4)
F6	−0.2337 (6)	0.5170 (4)	0.4359 (4)	0.097 (3)
P4	−0.1000 (2)	0.45945 (14)	0.16001 (10)	0.0349 (7)
F7	−0.1439 (4)	0.5320 (3)	0.2002 (2)	0.056 (2)
F8	−0.0547 (4)	0.3868 (4)	0.1188 (3)	0.075 (3)
F9	−0.0121 (6)	0.5257 (4)	0.1482 (4)	0.114 (4)
F10	−0.0128 (6)	0.4286 (5)	0.2240 (3)	0.114 (3)
F11	−0.1827 (6)	0.3930 (4)	0.1731 (5)	0.135 (5)
F12	−0.1819 (6)	0.4906 (5)	0.0948 (3)	0.113 (3)
CC1	0.5099 (7)	0.7359 (6)	0.2591 (5)	0.045 (3)
CC2	0.4700 (7)	0.7784 (5)	0.1986 (5)	0.040 (3)
CC3	0.4071 (7)	0.8537 (5)	0.1955 (4)	0.037 (3)
CC4	0.3878 (7)	0.8875 (6)	0.2533 (4)	0.038 (3)
CC5	0.4284 (8)	0.8448 (6)	0.3137 (5)	0.049 (4)
CC6	0.4912 (8)	0.7700 (6)	0.3168 (5)	0.047 (4)

[a] For anisotropic atoms, the U value is U_{eq} calculated as $U_{eq} = {}^1/_3\sum_i\sum_j U_{ij}a_i^*a_j^*A_{ij}$, where A_{ij} is the dot product of the ith and jth direct-space unit cell vectors.

Experimental Crystallographic Analysis. For each experiment a single crystal was affixed to a glass fiber attached to a goniometer head and then transferred to a Syntex $P2_1$ autodiffractometer, where it was maintained in a cold stream (−110 °C) of dry nitrogen gas for the duration of the data collection. Preliminary studies showed the crystal symmetries and their suitability for data collection. A summary of the preliminary studies and other details regarding data collection and processing are given in Table V. The measured intensities were reduced and assigned standard deviations as described elsewhere,[27] including correction for absorption based on crystal shape.

Solution and Refinement of the Structures.[27] Each structure was solved by the heavy-atom method (Patterson map). With the use of heavy-atom positions, the rest of the non-hydrogen atoms were found from subsequent electron density and difference density maps. Structure refinements were carried out by using full-matrix least-squares methods (SHELX76). Scattering factors[28] of the neutral atoms for H, C, N, O, F, P, S, Ni, Cl, and Pt were used, including real and imaginary corrections for anomalous dispersion. Non-H atoms were refined anisotropically, and H atoms were treated isotropically in all the structures. Phenyl rings were treated as

(27) Riley, R. E.; Davis, R. E. *Acta Crystallogr., Sect. B: Struct. Crystallogr. Cryst. Chem.* **1976**, *32*, 381. Computer programs used in the data reduction and in the structure refinement and analysis are as detailed in: Gadol, S. M.; Davis, R. E. *Organometallics* **1982**, *1*, 1607. (See the note at the end of the paper regarding the availability of supplementary material.)

(28) Scattering factors for H, C, N, O, F, Cl, P, and S atoms were used as programmed in SHELX76. Values for the Pt and Ni atoms were obtained from: *International Tables for X-ray Crystallography*; Kynoch: Birmingham, England, 1974; Vol. IV.

rigid groups, constrained with C-C = 1.39 Å, C-H = 1.00 Å, and C-C-C = C-C-H = 120°. Individual methylene groups were also treated as rigid groups with C-H = 1.00 Å and H-C-H = 109.5° throughout the refinement. However, the isotropic thermal parameters of these and all other hydrogens were allowed to refine independently. Details of the refinements appear in Table V.

Difference maps for the *t*-P_3S·NiCl structure indicated the presence of a disordered solvent molecule. The best agreement with difference maps was obtained by treating this disordered region as corresponding to CH_2Cl_2 with the two chlorine atoms having occupancies of 0.62 and 0.58, respectively. Tables VI-IX contain the fractional coordinates and the isotropic thermal parameters for the non-hydrogen atoms for the complexes containing the [*c*-PSPS·Ni^{II}], [*c*-P_3S·Pt^{II}], [*t*-P_3S·$Ni^{II}Cl$], and [*t*-P_3S·$Ni^{II}(NCCH_3)$] moieties, respectively.

During the structure analyses reported in this paper, it was discovered that the previously reported structure of *c*-PSPS·Pt[48] had been refined by using an incorrectly computed absorption correction. Final cycles of refinement have now been repeated with reflection data corrected by using the revised absorption coefficient, 40.12 cm^{-1} instead of 10.03 cm^{-1}. In this refinement, final $R = 0.050$, $R_w = 0.038$, and $S = 1.21$, compared to 0.053, 0.044, and 1.40, respectively, for the data as previously processed. The range of residual peaks in the difference map is now -1.40 to +1.30 e $Å^{-3}$, compared to a previous range of -1.68 to +1.53 e $Å^{-3}$. The new structural parameters are in good agreement with those previously reported. Differences in positional parameters were generally less than 1 esd, with occasional excursions up to 2 esd. Thus, there are no significant changes in the structural conclusions reported earlier. Table X presents revised fractional coordinates and isotropic thermal parameters for non-hydrogen atoms of the complex containing the [*c*-PSPS·Pt^{II}] moiety. As anticipated, thermal parameters were affected more, changing by up to 5 esd. Revised tables of structure factor amplitudes, atomic parameters, and bond lengths and angles appear with the supplementary material for this paper (see note at the end).

Acknowledgment. Financial support is gratefully acknowledged from the National Science Foundation (E.P.K., Grant CHE84-19282; M.A.F., Grant CHE85-09314) and the Robert A. Welch Foundation (E.P.K., Grant No. F573; R.E.D., Grant No. F233; M.A.F., Grant No. F677).

Supplementary Material Available: Listings of fractional crystallographic coordinates and isotropic thermal parameters for hydrogen atoms (Tables II, VI, X, XIV, and XVIII), anisotropic thermal parameters for non-hydrogen atoms (Tables III, VII, XI, XV, and XIX), and bond lengths and angles (Tables IV, VIII, XII, XVI, and XX) (for *c*-PSPS·Ni, *c*-P_3S·Pt, *t*-P_3S·NiCl, *t*-P_3S·Ni(NCMe), and *c*-PSPS·Pt, respectively) (21 pages); listings of observed and calculated structure factor amplitudes (Tables I, V, IX, XIII, and XVII) (for the compounds listed above, respectively) (198 pages). Ordering information is given on any current masthead page.

Contribution from the Department of Chemistry,
The University of Texas at Arlington, Arlington, Texas 76019-0065

Electronic Structure of the Ditelluromercurate(II) Zintl Anion. A Scattered-Wave-Xα Study

Frank U. Axe and Dennis S. Marynick*

Received October 15, 1986

The multiple-scattering Xα method along with quasi-relativistic corrections was used to study the electronic structure of the ditelluromercurate(II) Zintl anion. The bonding is found to have significant ionic character. Two key σ molecular orbitals comprise the skeletal bonds present in the anion. These bonding orbitals arise from the in-phase and out-of-phase combinations of the tellurium $5p_\sigma$ atomic orbitals with mercury 6s and 6p atomic orbitals, respectively. A destabilizing interaction between the mercury $5d_{z^2}$ atomic orbital and the in-phase combination of the tellurium 5s atomic orbitals occurs. The major effect of the relativistic corrections is the reduction of this destabilizing interaction. The remaining valence electrons are nonbonding. The localized valence structure of the $HgTe_2^{2-}$ anion is analogous to that found in dihalomercurate(II) systems.

Introduction

Initial investigations by Zintl[1] and co-workers in the 1930s presented strong evidence for the formation of polyatomic anions of post-transition-metal elements when the alkali-metal alloys of the post-transition-metal elements were dissolved in liquid ammonia or ethylenediamine. Attempts to isolate these species by evaporation of the solvent yielded only the original intermetallic phase. The first isolation and subsequent crystal structure of what are now commonly referred to as Zintl anions occurred in 1970.[2] Since then, Corbett and co-workers have structurally characterized a large assortment of homopolyatomic (i.e., Ge_9^{4-},[3] Sn_9^{4-},[5] Sn_5^{2-},[5] Pb_5^{2-},[5] Sb_4^{2-},[6] and Bi_4^{2-}[7]) and heteropolyatomic (i.e., $HgTe_2^{2-}$,[8] $Pb_2Sb_2^{2-}$,[9] $Sn_2Bi_2^{2-}$,[10] $Tl_2Te_2^{2-}$,[11] and $TlSn_8^{3-}$[12]) anions from the same general kinds of solutions described by Zintl over 30 years ago. The addition of a sequestering agent prior to evaporating the solvent is the key step in the isolation of these very elusive and unstable species. The use of the bicyclic 2,2,2-crypt[13] molecule in this regard prevents the reversion of the dissolved components back to the intermetallic phase upon evaporation by complexing the alkali-metal cations present in solution. Much of the background regarding the early work in the chemistry of Zintl anions is presented in an excellent review article[14] by Corbett. In addition to the numerous crystallographic studies, several systematic NMR investigations[15-18] have identified a number of Zintl anions in

(1) (a) Zintl, E.; Gonbeau, J.; Dullenkopf, W. *Z. Phys. Chem., Abt. A* **1931**, *154*, 1. (b) Zintl, E.; Harder, A. *Z. Phys. Chem., Abt. A* **1931**, *154*, 47. (c) Zintl, E.; Dullenkopf, W. *Z. Phys. Chem., Abt. B* **1932**, *16*, 183. (d) Zintl, E.; Kaiser, H. *Z. Anorg. Allg. Chem.* **1933**, *211*, 113.
(2) Kummer, D.; Diehl, L. *Angew. Chem., Int. Ed. Engl.* **1970**, *9*, 895.
(3) Belin, C. H. E.; Corbett, J. D.; Cisar, A. *J. Am. Chem. Soc.* **1977**, *99*, 7163.
(4) Corbett, J. D.; Edwards, P. A. *J. Am. Chem. Soc.* **1977**, *99*, 3313.
(5) Edwards, P. A.; Corbett, J. D. *Inorg. Chem.* **1977**, *16*, 903.
(6) Critchlow, S. C.; Corbett, J. D. *Inorg. Chem.* **1984**, *23*, 770.
(7) Cisar, A.; Corbett, J. D. *Inorg. Chem.* **1977**, *16*, 2482.
(8) Burns, R. C.; Corbett, J. D. *Inorg. Chem.* **1981**, *20*, 4433.
(9) Critchlow, S. C.; Corbett, J. D. *Inorg. Chem.* **1985**, *24*, 979.
(10) Critchlow, S. C.; Corbett, J. D. *Inorg. Chem.* **1982**, *21*, 3286.
(11) Burns, R. C.; Corbett, J. D. *J. Am. Chem. Soc.* **1981**, *103*, 2627.
(12) Burns, R. C.; Corbett, J. D. *J. Am. Chem. Soc.* **1982**, *104*, 2804.
(13) 4,7,13,15,21,24-Hexaoxa-1,10-diazabicyclo[8.8.8]hexacosane, $N(C_2H_4OC_2H_4OC_2H_4)_3N$.
(14) Corbett, J. D. *Chem. Rev.* **1985**, *85*, 383.
(15) Rudolph, R. W.; Wilson, W. L.; Parker, F.; Taylor, R. C.; Young, D. C. *J. Am. Chem. Soc.* **1978**, *100*, 4629.

0020-1669/87/1326-1658$01.50/0